Satyam Saini[1]
Mechanical and Aerospace Engineering Department,
The University of Texas at Arlington,
Arlington, TX 76019
e-mail: satyam.saini@mavs.uta.edu

Jimil M. Shah
Mechanical and Aerospace Engineering Department,
The University of Texas at Arlington,
Arlington, TX 76019

Pardeep Shahi
Mechanical and Aerospace Engineering Department,
The University of Texas at Arlington,
Arlington, TX 76019

Pratik Bansode
Mechanical and Aerospace Engineering Department,
The University of Texas at Arlington,
Arlington, TX 76019

Dereje Agonafer
Mechanical and Aerospace Engineering Department,
The University of Texas at Arlington,
Arlington, TX 76019

Prabjit Singh
IBM Corporation,
2455 South Road,
Poughkeepsie, NY 12601

Roger Schmidt
IBM Corporation,
2455 South Road,
Poughkeepsie, NY 12601

Mike Kaler
Mestex, A Division of Mestek Inc.,
4830 Transport Drive,
Dallas, TX 75247

Effects of Gaseous and Particulate Contaminants on Information Technology Equipment Reliability—A Review

Over the last decade, several hyper-scale data center companies such as Google, Facebook, and Microsoft have demonstrated the cost-saving capabilities of airside economization with direct/indirect heat exchangers by moving to chiller-less air-cooled data centers. Under pressure from data center owners, information technology equipment OEMs like Dell and IBM are developing information technology equipment that can withstand peak excursion temperature ratings of up to 45 °C, clearly outside the recommended envelope, and into ASHRAEs A4 allowable envelope. As popular and widespread as these cooling technologies are becoming, airside economization comes with its challenges. There is a risk of premature hardware failures or reliability degradation posed by uncontrolled fine particulate and gaseous contaminants in presence of temperature and humidity transients. This paper presents an in-depth review of the particulate and gaseous contamination-related challenges faced by the modern-day data center facilities that use airside economization. This review summarizes specific experimental and computational studies to characterize the airborne contaminants and associated failure modes and mechanisms. In addition, standard lab-based and in-situ test methods for measuring the corrosive effects of the particles and the corrosive gases, as the means of testing the robustness of the equipment against these contaminants, under different temperature and relative humidity conditions are also reviewed. It also outlines the cost-sensitive mitigation techniques like improved filtration strategies and methods that can be utilized for efficient implementation of airside economization. [DOI: 10.1115/1.4051255]

1 Introduction

With increasing demands for cloud computing, high-performance computing solutions, efficient thermal management of datacom facilities has become even more challenging [1–3]. A large fraction of energy and resources are expended for continuous cooling of the information technology equipment (ITE) to comply with special environmental requirements of temperature, humidity, and cleanliness for continuous reliable operation. Heat loads have become the defining characteristic and design criteria of data centers. This is evident from recent reports that projected 73 billion kWh of electricity consumption in 2020 [4]. These reports also estimated that because of the increased demand for information technology (IT) services, data centers alone accounted for an estimated 1.7%–2.2% of the total energy consumption in the U.S. and 1.1%–1.5% globally in 2010 [4,5]. When compressor-based air-cooling is used in data centers, the cooling power can account for approximately a third of total power consumption as seen in Refs. [6] and [7]. There has been, therefore, a constant effort to resort to cooling technologies that can generate considerable cost savings by cooling power reduction.

To address this concern of rising cooling power consumption, ASHRAE TC 9.9 expanded its recommended ranges for temperature and humidity to increase the number of hours for airside economization [8]. The recommended envelope in these guidelines specifies 18 °C–27 °C dry bulb temperature, −9 °C to 15 °C dew point temperature, and up to 60% relative humidity as shown in Fig. 1. The allowable envelopes in these guidelines also allow brief excursions outside the recommended envelope to the allowable envelopes where the datacom equipment can operate at a higher inlet dry bulb temperature of 45 °C and 90% relative humidity (RH). A reduction in cooling power consumption, thus, can be achieved by directly using outside air, using airside economizers to partially or completely cool down ITE heat loads under favorable conditions [9,10]. An airside economizer is typically

[1]Corresponding author.

Contributed by the Electronic and Photonic Packaging Division of ASME for publication in the JOURNAL OF ELECTRONIC PACKAGING. Manuscript received March 12, 2020; final manuscript received May 18, 2021; published online September 15, 2021. Assoc. Editor: Baris Dogruoz.

defined as "A duct and damper arrangement and automatic control system that together allows a cooling system to supply outdoor air to reduce or eliminate the need for mechanical cooling during mild or cold weather" [11]. Free air cooling is implemented when the amount of enthalpy in the air is sufficient and no additional conditioning is required for sufficiently cool and dry [12]. Figure 2 is a schematic showing the working of an airside economizer unit utilizing direct/indirect evaporative cooling.

The reluctance in the implementation of airside economization from data center owners is due to the increased risk of exposure of ITE to particulate and gaseous contaminants. These contaminants can enter the data center either directly in the economizer mode or indirectly through media such as low-efficiency filters and makeup air. A study from Intel concludes that for 10 months in a free air-cooled data center, the humidity can vary between 4% and 90%. Since there is a minimum control over temperature, humidity, and airborne contaminant introduction in economizer mode, the ITE reliability can be easily compromised [13]. Among the airborne contaminants, highly reactive gases, and low deliquescence relative humidity (DRH) value particles are of primary concern. Gases like H_2S, Cl_2, NO_2, SO_2, and O_3 have been identified to be most corrosive for electronics in presence of favorable temperature and humidity conditions [14]. Details on underlying failure modes and mechanisms due to these contaminants will be provided in the later sections of this paper. In presence of such contaminants, the surrounding environmental parameters of temperature, RH, and contamination can cause ITE failures via two main mechanisms. The first is electrical open circuits due to corrosion of silver terminals in surface mount resistors in the corrosive environment of sulfur-rich gases. The second common failure mode is due to copper creep corrosion causing electrical open circuits due to electrochemical migration (ECM) or cathodic-anodic filamentation [15–19]. These corrosion mechanisms and the rate of corrosion in any given environment can be affected by temperature, humidity, and level, and type of particulate and gaseous contaminants [20–23]. The above-mentioned failure modes also led to new specifications for contamination limits accepted by the industry, which now place a lower limit on the DRH of dust [24,25].

To better understand these failure modes associated with data center particulate and gaseous contamination, it is essential to understand the relationship between environmental RH and settled the hygroscopic matter on the printed circuit boards (PCBs). Airborne particulate matter and hygroscopic gaseous corrosion products are known to become wet and therefore ionically conductive and corrosive if the humidity in the environment rises above the DRH of the particulate matter. It is, therefore, necessary and informational to have a clear understanding of the terms critical relative humidity (CRH) and DRH. CRH is the value of the relative humidity at which the settled particulate matter starts adsorbing enough moisture to become electrically conductive. Whereas the relative humidity value at which the settled particulate matter becomes completely aqueous is termed as the DRH for the settled particle mixture. When the RH inside the data center, locally or globally, exceeds the DRH value of salts or accumulated particles on the PCB, the subsequent conductive solution formed leads to electrical short-circuiting due to a reduction in surface insulation resistance (SIR) between the closely spaced features on the PCBs [26].

There is a wide body of experimental literature and review articles on the mechanism of corrosion and associated failure modes in electronic packages and materials. Similar work on the effect of particulate and gaseous contamination in data centers and electronic failures is not available. The primary motivation behind this study is to carry out a systematic review of literature on the effects of particulate and gaseous contaminants on equipment reliability in data centers where airside economization or free air cooling is the primary mode of cooling. This paper reviews the experimental and computational literature on failure modes and mechanisms related to settled hygroscopic matter and gaseous contaminants. The paper is divided into four main sections. It begins by reviewing essential literature related to the data center and airborne contaminants classification and their sources. An introduction to the related failure modes and the parameters influencing them is then provided with relevant reviewed literature. This is followed by a review of experimental and computational research on both gaseous and particulate contamination. An outlook on the reviewed literature is also presented to discuss the gaps in the literature in terms of lack of available data and in-situ

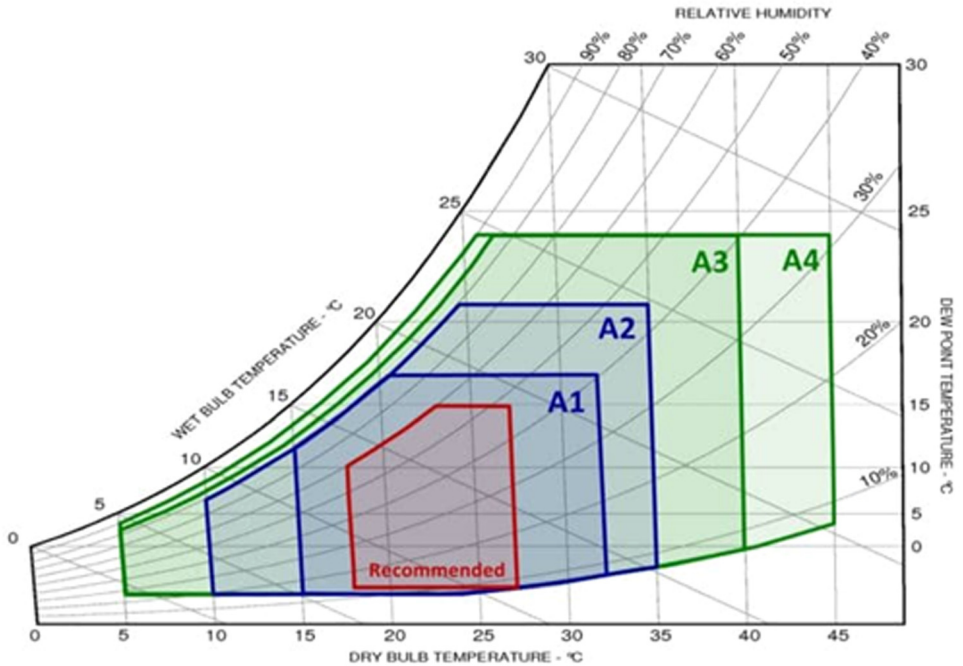

Fig. 1 ASHRAE 2015 environmental guidelines showing the recommended and allowable ranges for temperature and humidity for data centers

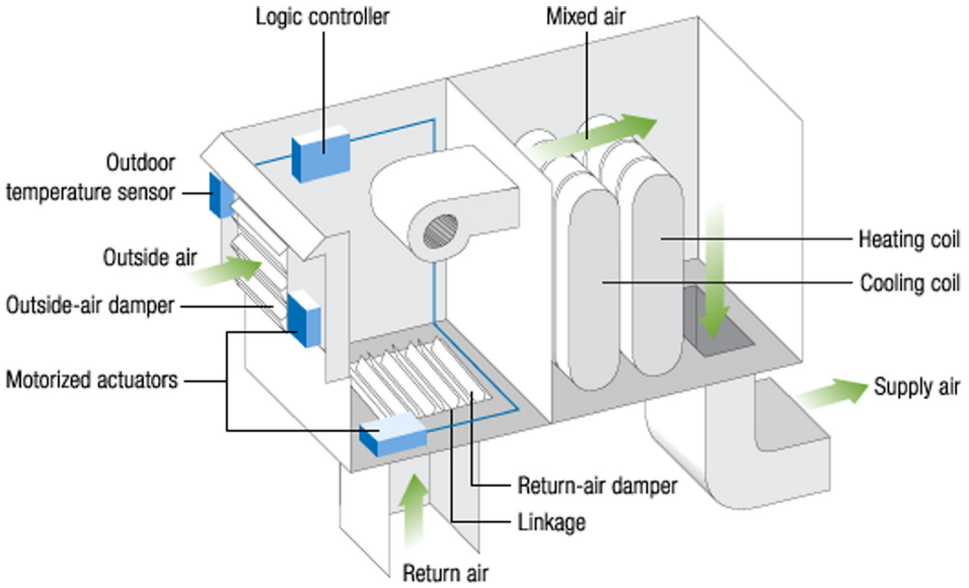

Fig. 2 A schematic of direct and indirect evaporative cooling unit/airside economizer

studies on the issue of data center contamination. Related topics of particle behavior and the underlying corrosion chemistry are beyond the scope of this paper and, therefore, have not been discussed in detail.

2 Sources of Contamination

The environment surrounding and within a server is defined by temperature, humidity, and gaseous and particulate contamination in the air [27,28]. In economizer mode, it is easier for these contaminants to enter the data center white space and cause ITE failures, under favorable conditions and over time. However, there is not adequate literature and statistics available directly correlating the impact of outdoor/indoor contaminant concentrations and ITE failure rates in data centers. To understand the failure mechanisms associated with data center contamination, it is equally imperative to identify the contamination sources. The first part of this section provides an overview of the pervasive gaseous contaminants and the second about particle contaminants and their sources.

2.1 Sources of Gaseous Contaminants. Gaseous pollution today is caused primarily by fossil fuel burning, factories, commercial and domestic buildings, and automobiles. Over the years, three main pollutant gases found are throughout the industrialized world: sulfur dioxide (SO_2), ozone (O_3), and nitrogen dioxide (NO_2). Other gaseous contaminants of primary concern include chlorides (chlorine [Cl_2] and hydrogen chloride [HCl]), acetic acid (CH_3COOH), and formaldehyde (HCHO) [29]. The types of gases that most commonly result in ITE corrosion are acidic gases such as hydrogen sulfide, sulfur, and nitrous oxides, and hydrogen fluoride; caustic gases, such as ammonia; and oxidizing gases, such as ozone. Out of the three, acidic gases are of interest. It should be pointed out that, sulfur-bearing gases like SO_2 (sulfur dioxide) and H_2S (hydrogen sulfide), the major gaseous contaminants, are not directly responsible for corrosion but, in fact, by combining with NO_2 (nitrogen oxide) and O_3 (ozone) make the product with the former two gases more corrosive [29]. ASHRAE 1775-TRP (2015) [30] provides the details about typical values of the outdoor concentrations of these gaseous contaminants worldwide as seen in Table 1. These values can vary by location and time of the year. Similar guidelines and pollutant classification are provided in ANSI/ISA-71.04-2013 for the most pervasive gaseous contaminants. These guidelines are classified based on the severity level affecting the ITE. As seen from Tables 1 and 2, the values suggested by ASHRAE are around the same magnitude as the ISA guidelines for ITE. Although, these values represent the absolute impact of the gaseous pollutants on ITE corrosion rates without considering their synergistic effects. An estimate of the worldwide surface concentration levels for SO_2 was presented by Buchard et al. [31] over 10 months. As seen in Fig. 3, the value of this concentration lies around the 40 ppb (parts per billion) mark which is similar to that given by ASHRAE 1775 TRP (2015). It is also seen that the concentration is higher during the winters, which also corresponds to the time for maximum economizer hours.

Table 1 ASHRAE RFP 1755-TRP typical outdoor pollutant concentrations worldwide

	Outdoor concentration in ppb	
Pollutant	Minimum	Maximum
H_2S	4	140
NO_2	5	80
SO_2	4	40
Cl_2	1	10
O_3	5	60

2.2 Sources of Particulate Contaminants. Particulate matter or dust is primarily classified into two groups: fine particles and coarse particles. Fine particles are defined as particles with a diameter less than or equal to 2.5 μm such as those found in diesel

Table 2 Contaminant concentrations versus severity levels (ANSI/ISA-71.04-2013)

	G1 (Mild)	G2 (moderate)	G3 (harsh)	GX (severe)
Gas	Concentration (ppb)			
H_2S	<3	<10	<50	50
SO_2, SO_3	<10	<100	<300	3000
Cl_2	<1	<2	<10	10
NO_x	<50	<125	<1250	1250
HF	<1	<2	<10	10
NH_3	<500	<10,000	<25,000	25,000
O_3	<2	<25	<100	100

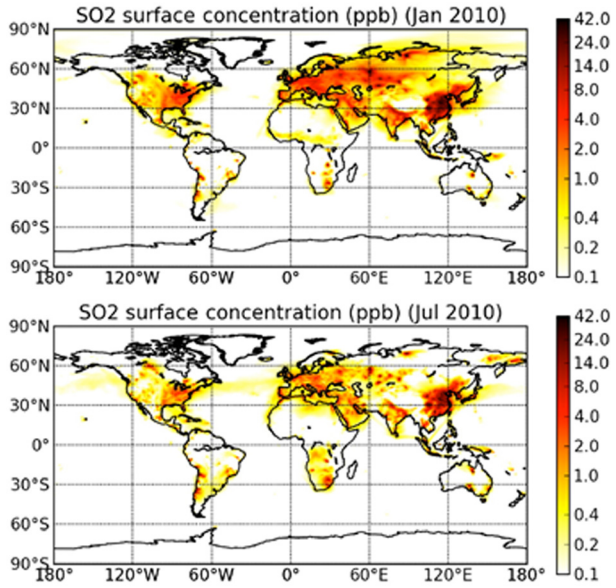

Fig. 3 Goddard earth observing system version 53GEOS-5/GOCART monthly mean of SO_2 surface-level (revised run) for January and July 2010 [31]

particulate matter, motor vehicle exhaust, and smog. These fine particles are further classified into primary and secondary particles [32,33] where primary particles are those that are directly emitted from a specific source, such as volcanoes, forest fires, and construction sites. Secondary fine particles are formed because of photochemical reactions that take place in the atmosphere and make up most of the fine particulate pollution. These photochemical reactions occur due to the presence of oxides of sulfur and nitrogen that are emitted from automobiles and various industries. Carbonaceous material with a size of fewer than 0.1 μm interacts with nitrogen dioxide and sulfur dioxide in a multistep photochemical process to result in the formation of nitric and sulfuric acids. Fertilizers generally containing ammonia, decayed biological matter, and other sources neutralize these acids thereby forming ammonium sulfate, ammonium nitrate, and ammonium hydrogen sulfate [34–38].

Coarse particles are typically related to a particle diameter range of 2.5–15 μm. They include particulate matter such as sea salts, natural and artificial fibers, and plant pollen. Their major sources mainly include erosion of soil, flaking of biological materials, and minerals which are accelerated by winds [39]. The sea salt particles get airborne due to a mechanism known as sea spray, where the salts become airborne as aerosol particles. These particles are also capable of reacting with other pollutant molecules to form new salts and dissociate into free ions. Within the data center, coarse particles can also be found in the form of zinc whiskers from the undersides of the floor tiles or metallic ducts electroplates with zinc. This form of particles is, although, considered to be rare. Another such rare source of indoor particles can be the salts entering the airstream from humidifiers. The reason behind this can be the high salt content in feedwater, especially the salts with low DRH values. It can be concluded from these studies that most of the contaminants, both gaseous and particulate, originate outdoors from either manmade or natural causes. A particle pollution report by Environmental Protection Agency analyzed and reported $PM_{2.5}$ and PM_{10} levels for 4 years [40]. The major findings of the report suggest that the majority of $PM_{2.5}$ is attributed to regional pollution due to sulfate, volatile organic compounds, and nitrate emissions from power plants and highways. This airborne particulate matter can be transported hundreds of miles away from the sources. This is consistent with the findings of one of the studies reviewed later in this paper which characterizes the dust found in a modular data center located in a polluted industrial area of Dallas, Texas. A summary of the particle origin found at this data center is shown in Table 3 [41]. The table summarizes the contaminants and their sources that might not be necessarily present in all economizer-based or free air-cooled data centers. It does, however, provides a good method of root causing and mitigating the particle origin sources, if particles of similar chemistry are found in a data center. Also, most of the particle sources summarized here are due to natural sources and can be mitigated if proper air filtration strategies are implemented. Section 3 will review the studies describing the most common failure modes and their mechanisms due to corrosive airborne or settled hygroscopic contaminants.

3 Contamination Failure Modes

This section discusses the literature on primary failure mechanisms associated with reliability degradation in free air-cooled data centers due to particulate and gaseous contaminants. Based on the reviewed literature, the failure modes were identified to be ECM, corrosion of silver terminals on PCBs and copper creep corrosion. These failure modes are particularly due to the contaminants discussed in the above section as concluded from the reviewed literature. The review of these failure modes is based on the data center cooling point of view and does not address the microscopic level mechanisms or morphological behavior of the discussed failure modes.

3.1 Electrochemical Migration. Electrochemical migration is a phenomenon that creates an electrical bridge between two conducting routes on the PCBs in the presence of certain contaminants under well-known environmental and electrical field conditions. This phenomenon causes the formation of dendrites between the energized wiring routes, thus, reducing SIR between them causing high leakage currents and PCB electrical failures. SIR is generally used to depict the reduction of resistance between closely spaced electrodes due to the presence of contaminants [42]. The resistance referred to in the SIR definition is the resistance of the insulating material between the electrodes. A reduction in this resistance, in presence of hygroscopic ionic contaminants, causes a leakage current between two adjacent electrodes, leading to failure in electronics. The factors influencing ECM are temperature, RH, wire spacing, materials, electric field, and type of contamination [43]. The threat of ECM is more in the electronic components that are not conformally coated to seal them against contamination. In such a case, the dust particles deposited on PCBs may lead to electrical short circuits via ECM.

The ECM process consists of four steps: (1) electrolyte layer formation, (2) ion accumulation, (3) ion transport, and (4) ion deposition or dendrite growth [43]. The typical mechanism of ECM and dendrite formation is shown in Fig. 4 [44] for an Sn solder alloy joint. The study describes that the electrolyte layer formation is further dependent on RH, contaminant presence, and

Table 3 Sources of some typical airborne contaminants [41]

Contaminant	Source
Zinc-whisker	Zinc coated ICT, steel building studs
Tin-whisker	Components and products with electroplated tin
Oxide flake off	Magnetic media
Natural and artificial fibers	Paper, cardboard, etc.
Water-soluble ionic salts	Chemical reaction
Sulfates, nitrates, and sea salts	Wind
Lime dust with water	Concrete material
Dust	Farms (especially during plowing)
Toner dust	Toner
Smoke	Cigarette, wind
Cellulose fragments	Traditional ceiling tiles and space

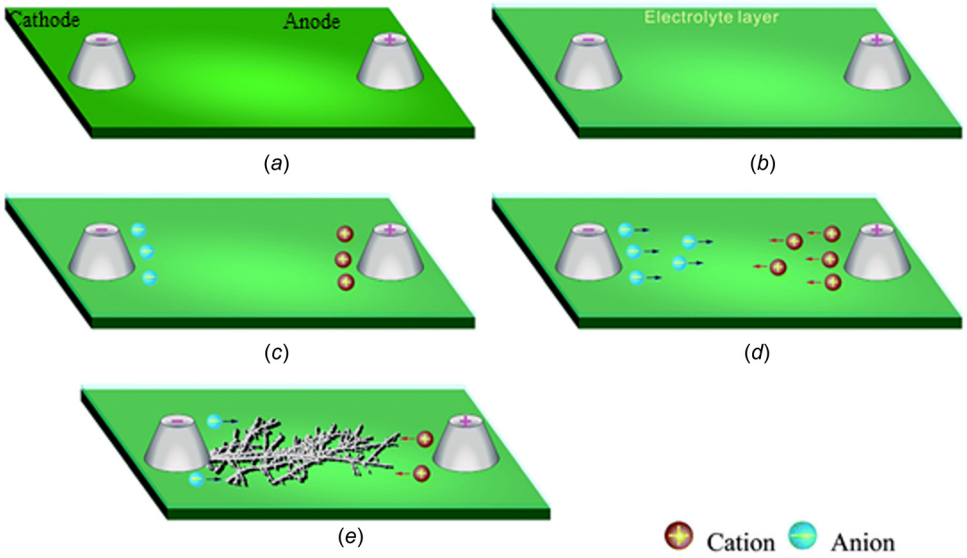

Fig. 4 The schematics of Sn solder alloy joints (*a*) ECM sample, and ECM process, (*b*) electrolyte layer formation, (*c*) dissolution of metal, and (*d*) ion transport and deposition of metal ions (dendrites growth)

temperature. It is also pointed out that these parameters can affect the ECM process independently of other parameters. For example, given a constant value of RH, with an increase in temperature, the absolute water content in the air increases, the adsorbed moisture on PCB surfaces will be higher, accelerating the dendrite formation and ECM. Similarly, with increasing RH, the thickness of the aqueous layer adsorbed on the PCB increases and so does the water absorption at the internal interfaces. Under the same bias voltage, the narrower the wire spacing, the shorter will be the ion migration path to be bridged by ECM-generated dendrites [44].

There is a voltage threshold that needs to be exceeded for ECM to occur and the total time to failure of PCBs by ECM is a power function of the electric field [45]. This means that potential bias has more contribution to ECM than wire or electrode spacing. Silver has amongst the highest propensity for ECM followed by Pb, Cu, Ni, and Au. This is due to low activation energy to initiate the ECM and higher anodic solubility of silver. An in-depth review has been conducted on ECM of metals such as Ag [46–50], Sn and Sn solder alloys [51–55], Cu [56–61], and other metals used in electronics [62–64]. These studies not only discuss the failure modes and dependence of ECM on the accelerating parameters but also provide insights into the associated transport mechanisms and reliability analysis using analytical models [60]. Another important finding from these studies, especially from the data center operating conditions point of view, is the acceleration of ECM due to the presence of chloride ions. For chloride-containing hygroscopic particulate matter, an RH of even 40% is sufficient to form various electrolyte monolayers [65,66]. This can be particularly detrimental from the ITE reliability point of view as this RH value lies within the ASHRAE recommended cooling envelope as discussed earlier.

3.2 Corrosion of Silver. Silver is sometimes used as a plating for electrical contacts on PCBs and is often used as a termination metal for surface mount resistors. Corrosion of resistor terminals can cause resistor failure by increasing the resistance due to the removal of corroded conductive material. The use of silver in electronic components has always been a source of concern due to its high propensity for ECM [67–69]. Additional test requirements are prudent if silver is used in electronics or it can be alloyed with noble metals to reduce its tendency for ECM [70,71]. Corrosion of silver, also known as silver tarnishing, is a well-studied subject by museums [72–74]. As per the reviewed literature, silver readily reacts with sulfur to form a nonconducting film of silver sulfide that causes an open circuit [75]. The initiation of sulfidation is through the reduction of H_2S or CoS to HS^-. In an aqueous solution, HS^- can then either react directly with silver ions that have oxidized, or they can be absorbed by surfaces, subsequently reacting to form the sulfide salt. The presence of oxidizing species, such as Cl, has been shown to increase the corrosion rate. A white paper from ASHRAE recommends that data center environmental corrosivity levels be such that copper and silver will corrode at rates less than 300 and 200 Å/month, respectively, to minimize the corrosion impact on ITE reliability [76]. These values were chosen based on the findings from an unpublished worldwide survey by ASHRAE which concluded that data centers with copper and silver corrosion rates <200 Å/month had a lower probability of ITE failures [77]. The gaseous environment classification system for users and manufacturers of electronic equipment has been classified by the ANSI/ISA-71.04 standard and is shown in Fig. 5 [78]. This standard is an effective and convenient way to quantify the indoor gaseous corrosivity level using reactivity monitoring that will be discussed in the latter part of this paper.

The robustness of thick film resistors which typically use silver termination can be improved by making the passivation layers covering the resistor elements more impervious to sulfur gases. This can be done by either using alternatives to silver such as silver alloys or noble metals to decrease the susceptibility to sulfur-induced corrosion. Several authors have documented the mechanism for silver sulfide corrosion of thick film resistors [79], as well as techniques for performing accelerated laboratory testing. These laboratory techniques include mixed flowing gas (MFG), hydrogen sulfide (H_2S) gas, sulfur oil, and flowers of sulfur exposures. Work remains to correlate the test results to the actual contamination levels in the field. Appropriate test methods could also assess well the mitigation techniques affect resistor reliability in a sulfur environment.

3.3 Copper Creep Corrosion. Copper creep corrosion is the corrosion of copper plating to copper sulfide on printed circuit boards and the creep of copper sulfide over the printed circuit boards, electrically shorting adjacent circuit-board features. Figure 6 shows an example of copper corrosion caused by dust settled on a printed circuit board [76]. In 2006, because the European Union's restricted hazardous substance (RoHS), the PCB failure rates due to creep corrosion increased dramatically for

ISA STANDARD S71.04-1985 WITH REVISED CHANGES			
CLASS	AIR QUALITY CLASSIFICATION	COPPER CORROSION	SILVER CORROSION
G1	MILD-Corrosion is not a factor	<300 A / 30 DAYS	<200 A / 30 DAYS
G2	MODERATE-Corrosion is measurable	<1000 A / 30 DAYS	<1000 A/ 30 DAYS
G3	HARSH-High Probability that corrosion attacks will occur	<1000 A / 30 DAYS	<2000 A/ 30 DAYS
GX	SEVERE-electronic/electrical equipment is not expected to survive	>2000 A / 30 DAYS	>2000 A/ 30 DAYS

Fig. 5 Gaseous corrosivity levels as per ANSI/ISA-71.04 guidelines (ISA 2013)

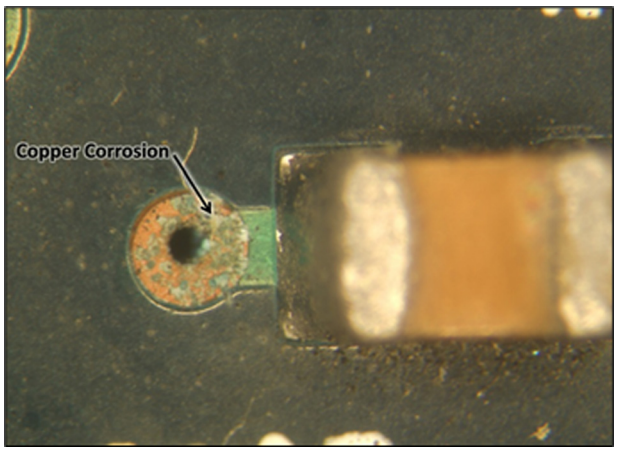

Fig. 6 Corrosion of a plated through-hole because of wetted ionic dust high in magnesium chloride

PCBs made from lead-free materials [80]. The typical Pb-Sn solders were replaced by Sn-Ag-Cu solder, also known as SAC. The SAC solder is shown to have poor copper metallization wettability as compared to Pb-Sn solder on PCB. The atmospheric corrosion mechanism of electronic materials and other cases of atmospheric corrosion are similar, as they are all affected by synergies between relative humidity [81–84], temperature [85,86], contaminants (Cl^-, H_2S, SO_2, and NO_x) [87–93] among others. The increase in creep corrosion due to the electronic industry moving away from Pb-free solders has been reported by several authors [94–96]. These studies mainly addressed that a move to ImAg and organic solderability preservatives (OSP) board finishes would dramatically increase early life failure in computer PCBs due to copper creep corrosion, especially in high sulfur environments. The creep corrosion on such surfaces is generally enhanced in presence of high humidity and temperature. It might be easier to control these environmental parameters in a data center where vapor compression-based cooling is used. But these finishes might suffer accelerated corrosion in free air-cooled conditions, where there are uncontrolled temperature and humidity transients.

There are various studies published which demonstrate the corrosion of copper in a laboratory environment using MFG tests [97–100]. These studies conclude that RH, sulfur dioxide, and hydrogen sulfide are the most influencing factors on the rate of copper corrosion [101]. Various other studies also demonstrate that apart from several atmospheric factors, relative humidity plays a major role in the corrosion of copper. Sulfur gases are the dominant reactive pollutants [102]; however, some reference is given to humidity and chlorine-containing gases as accelerators of corrosion [103]. The formation of tarnish films on a copper surface exposed to environments containing atmospheric pollutants and high humidity involves the movement of metallic ions over the surface, away from the metal, generating a creeping process that increases the contact resistance, leading to electric failures of the electronic devices [104]. Copper sulfidation is a fast process occurring on the metal-gas phase interface impairing the copper corrosion resistance [105,106].

4 Experimental Studies on Gaseous Contamination

To thoroughly understand the effects and mechanism of corrosion due to gaseous contamination, several laboratory experimental procedures have been developed. These accelerated procedures aim at simulating near similar environmental conditions in laboratory facilities, which help researchers and data center administrators to understand the root causes of field failures and prevent such future field failures. Mixed flowing gas and flowers of sulfur (FoS) are the two most popular testing methods to determine electronic equipment reliability in harsh environments. These tests are mainly used to quantify the PCB reliability with various surface finishes for Pb-free solders. Based on the reviewed literature, immersion silver (ImAg), immersion tin (ImSn), OSP, electroless nickel immersion gold (ENIG), and hot air solder leveling have been studied widely in harsh laboratory and field environments. The subsections in Sec. 4 summarize these methods and review some of the earliest and latest works utilizing these methods. The popular and most widely used in-situ method of reactivity monitoring or corrosion classification coupon testing for gaseous contaminants is also discussed.

4.1 Mixed Flowing Gas. A mixed flowing gas test is used to simulate the corrosion phenomenon due to atmospheric exposure. Development of the industry-standard MFG test started in the 1980s at Battelle Labs, which carried out tests on the use of MFG to accelerate atmospheric corrosion and its effect on electronic components [107–109]. In the 1990s, professional organizations, including the American Society for Testing and Material (ASTM), Electronic Industries Association (EIA), International Electrotechnical Commission (IEC), and Telcordia, began to standardize these test methods and published procedures and guidelines. The operational environments for electronic equipment in the atmosphere were divided into four classes, from the least corrosive (class I) to the most corrosive (class IV) as shown in Table 4. This table provides the overall summary of the dominant corrosion products and dominant corrosion mechanisms that can be expected in each of these environmental classifications from field data. class-I depicts a well-controlled office environment with continuous adjustment. Whereas, class-II shows a light industrial environment, such as business offices without effective or continuous environment control. Class-III is a moderate industrial environment, such as storage areas with poor environmental control, and class-IV is heavy industrial environments, such as locations adjacent to primary sources of atmospheric pollutant gases.

The primary challenge, as discussed by Abbott, regarding the development of the MFG test was difficulty in comparing and

Table 4 Definition of environmental classes by dominant mechanism(s) and chemistries on control coupons [109]

	Au/Ni/Cu (Porous)		Copper
Class	Mechanism	Highest to lowest	Chemistry
I	None	–	Cu_2O
II	Pore	Ni, Cu, Cl, O, (S)	Cu_2O, $Cu_xO_yCl_z$
III	Pore and creep	Cu, S, Ni, Cl, O	Cu_2S, Cu_2O, (?)[a]
IV	Creep	Cu, S, Ni, O, Cl	Cu_2S, (Cu_2O), (?)[b]

[a]? and
[b]? indicate unknowns, ( ) indicates minor amounts (<10%).

lack of availability of indoor environmental data. The problem was partially resolved by reactivity monitoring in the late 1970s [110]. His study presented the significance of this technique, showing reactivity distributions for copper as shown in Fig. 7 and the following important principles:

(1) Real indoor environments for electronics may differ by at least four to five orders of magnitude in chemical severity [111,112].
(2) The degree of exposure/risk of severe versus benign applications differed widely among manufacturers, even within the same industry.
(3) At least four fundamentally different classes of field environments may be demonstrated.

The study concluded that in all the cases considered, relative humidity, reactive chloride concentration, and reactive sulfide concentration were consistently identified as the most detrimental factors attributing to corrosion. The impact of temperature, gas velocity, and NO_2 concentration was concluded to be far less critical. SO_2 was also shown to be relatively unimportant for indoor, field, and/or laboratory mixtures. It was concluded that three-component mixtures based upon low levels of H_2S, NO_2, and Cl_2 could be used to satisfy the simulation of all reactive environmental classes.

Zhang et al. [113] studied the corrosion of immersion silver (ImAg) finished copper land patterns on PCBs due to SO_2 exposure in a mixed flow gas chamber. Six test conditions were examined with varying concentrations, temperatures, relative humidity, and exposure times. The test samples were suspended in the MFG test chamber using insulated wires. Visual inspections were conducted during the exposure using an environmental scanning electron microscope (ESEM), and after removal from the experimental chamber the elemental composition of each specimen was measured by energy dispersive spectrometry (EDS). The results show that there were two mechanisms of corrosion for ImAg-finished PCBs in an SO_2 gas environment: direct chemical corrosion and electrode reaction. There was no evidence that Ag_2S and Cu_2S or CuS were produced in the corrosion products. Under high humidity, chemical and electrode reactions both existed, and the corrosion products could include Ag_2O, AgCl, Ag_2SO_3, CuO, $CuCl_2$, and CuCl. With low humidity, the chemical corrosion was predominant, and the corrosion products could include Ag_2O, CuO. Passive films of the corrosion products were formed on ImAg finished surface under long exposure time. These passive films also prevented further corrosion on the ImAg surface in the MFG chamber. Additionally, the temperatures within the range of 30 °C–40 °C did not have any obvious influence on the ImAg-finished PCBs.

Cullen [114] reproduced creep corrosion using a condensing vapor test, that created H_2S by adding 1% hydrochloric acid to 0.1 g/l sodium bisulfide. Every finish considered in the study exhibited creep corrosion in this environment within 24 h. The

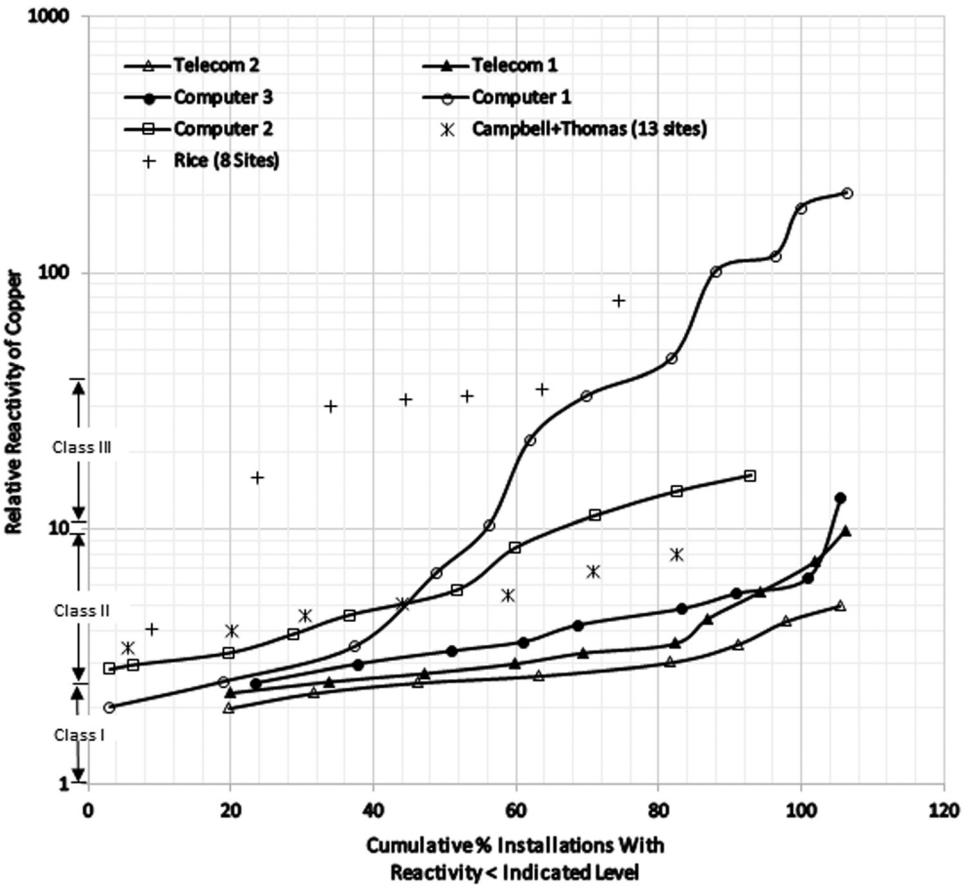

Fig. 7 Typical reactivity distributions for individual manufacturers and/or product lines

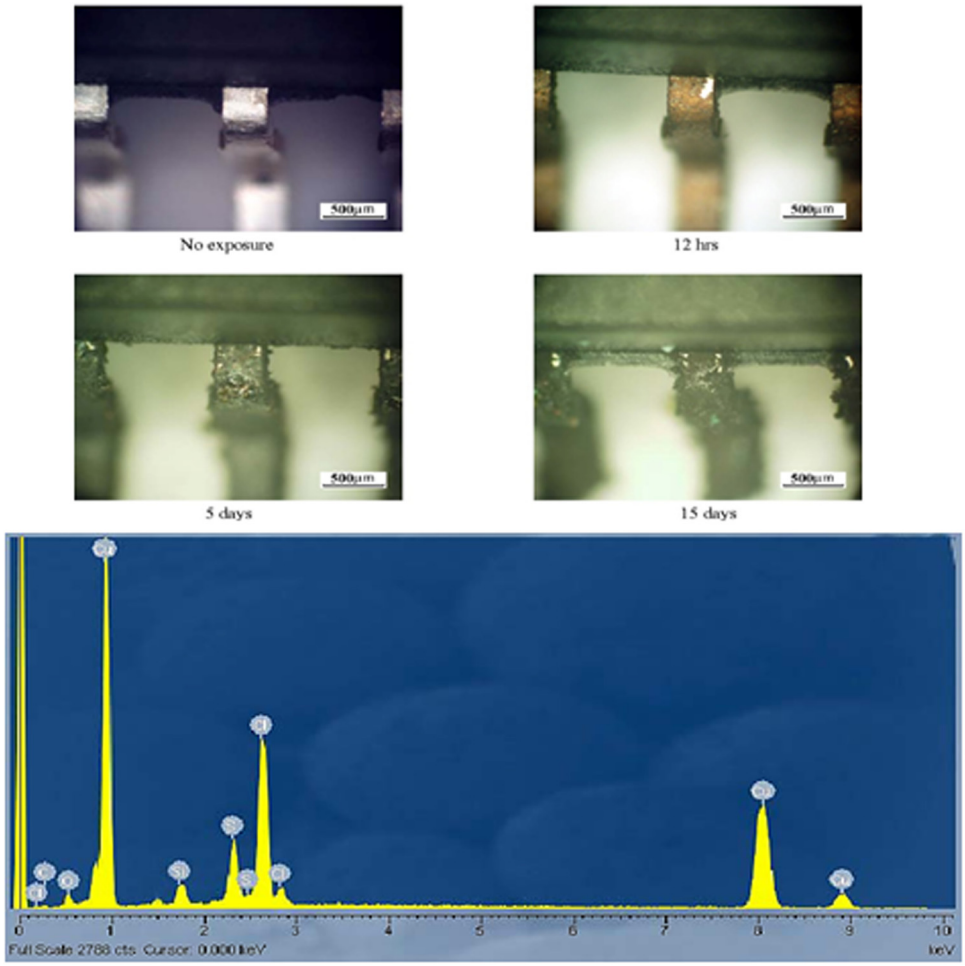

Fig. 8 (Top) ESEM view of creep corrosion over molding compound surface and leading-edge area on QFN package with Ni/Pd/Au–Ag finish (type 7) after 15 days of MFG exposure. (Bottom) EDS analysis showing various elements present in the corrosion products formed, the majority being Cu, S, Cl, and O.

authors also conducted class III MFG testing and found no occurrence of creep corrosion until an RH value of over 93% was reached. Veale [115] conducted MFG testing with (100 ppb H_2S; 200 ppb NO_2; 200 ppb SO_2; 20 ppb Cl_2) with temperature and humidity values of 29 °C and 75%RH. The test duration was 20 days or 480 hours. The objective of the study was to investigate the corrosion resistance of finishes like OSP, ImAg, ENIG, and ImSn. The test progress was monitored by analyzing the accumulation of the copper corrosion layer which was 3500 Å/day, which corresponds to ISA G1 (or Battelle class III). The study concluded that none of the coatings tested were immune to failure in a Battelle class III environment. It was also concluded that the finishes ImSn and OSP could survive in a Battelle class II environment [116].

In another study by Xu et al. [117], MFG testing was conducted on PCBs with OSP, ImAg, ImSn, and ENIG finish. A more severe environment representing Battelle class IV and ISA class G2 conditions (1700 ppb of H_2S, 200 ppb of NO_2, 20 ppb of Cl_2, and 200 ppb SO_2) was considered where the temperature was kept at 40 °C with an RH value of 69%. These conditions represent the worst-case outdoor concentrations for these contaminants as discussed in Sec. 2. After 48 h, it was observed that all the ImAg finishes had a grayish corrosion product, mostly Cu_2S. Out of the seven ImAg finishes tested, four finishes, after 5 days of exposure in the MFG chamber, showed fiber-assisted ECM, and another sample showed the same type of corrosion after 10 days. The results concluded that the boards with ImAg finish corroded mores than the other three types of finishes tested. Another issue that was associated with ImAg was the peeling of the conductive corrosion products from the surfaces. The flaking or peeling was minimal until 10 days after the test but became more prominent after 40 days of exposure in the MFG chamber.

Copper creep corrosion using a noble metal finish was analyzed by Zhao et al. on preplated lead frame packages [118]. For quality and reliability assessment of the packages, they were exposed to various ECM testing using an MFG chamber as seen in Fig. 8. The testing was done on standalone packages as well as by integrating them on the PCB for analyzing the reflow soldering effect and were compared with SnPb plated lead frame packages. The packages were exposed to three different types of conditions. For the four types of packages subject to three types of extreme conditions with temperature/RH values of 40 °C/93% for 168 hours, 65 °C/88.5% for 500 hours, and 85 °C/88.5% for 168 hours in accordance to IPC-TM-650 method 2.6.14.1 standard. After the exposure, no ECM failure was observed from a resistance drop point of view, but creep corrosion occurred on all test samples in the Battelle class III environment. Significant corrosion was observed after 15 days on packages as shown in Fig. 8. Another observation made was that there was no compelling difference between the corrosion appearance of the various samples tested. Lesser corrosion was observed on SnPb plated quad-flat no-leads (QFN) than the QFN package with Ni/Pd/Au-Ag finishes. On the mold surface, creep corrosion occurred within eight days of exposure on the QFN packages with the Ni/Pd/Au–Ag finish. Dendritic

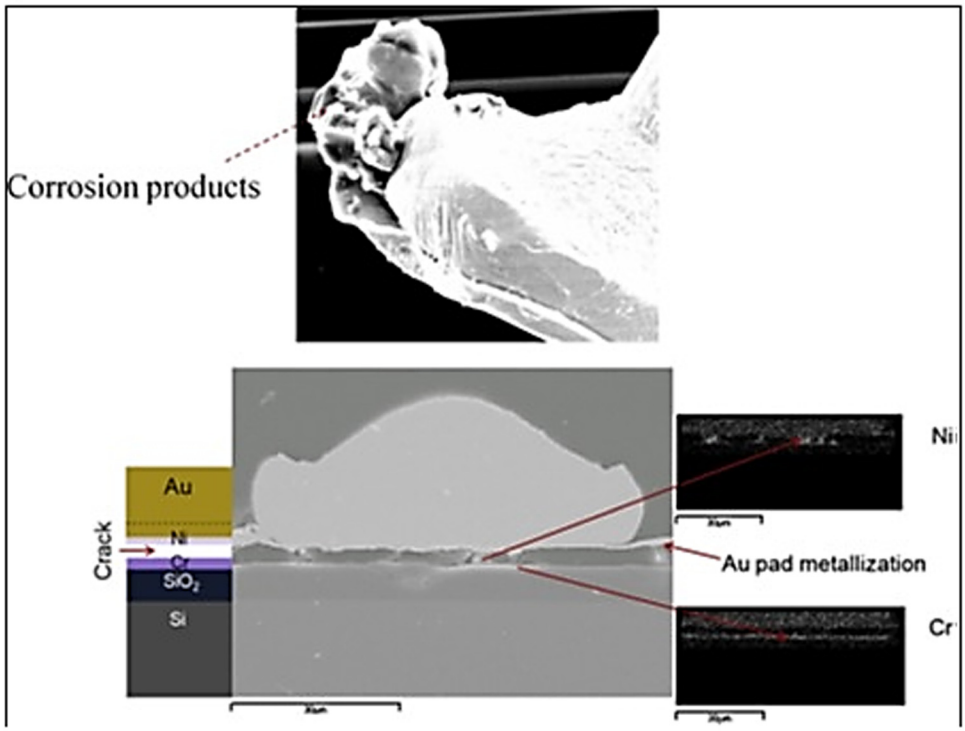

Fig. 9 (Top) SEM image of a detached wire bond that had experienced 90 days mixed flowing gas test. (Bottom) A cross section image of a tested wire bond and EDS analysis.

Table 5 Parameters used in the mixed flowing gas test and typical nordic outdoor environments [120]

Environment	° C	%RH	Cl_2 ($\mu g/m^3$)	H_2S ($\mu g/m^3$)	NO_2 ($\mu g/m^3$)	SO_2 ($\mu g/m^3$)
Test chamber	30	70	19	263	188	136
Outdoor (nordic)	5	78	0.9	4.6	28	30

formations of creep corrosion products were observed on the mold compound which can cause electrical bridging of adjacent traces. As per the acceleration factor relation by Williams [119], eight days of testing as per the Battelle class III test conditions correspond to about four years of field operation or storage in an industrial environment.

Jue et al. [120] demonstrated the MEMS reliability of a microphone by conducting accelerated testing using MFG and shock impact testing as shown in Fig. 9. The gaseous species concentration in lab experimental chambers is typically 4–40 times higher than those in typical Nordic outdoor environments as shown in Table 5. For this study, after 90 days of exposure in the MFG chamber, corrosion in the wire bond and wire bonds and membrane cracking due to membrane embrittlement was observed. This was attributed to the fact that the diffusion of Ni through the pad's metallization could have caused an increase in the corrosion products in the wire bonds and subsequent detaching. A possible way of mitigating such an issue could be using Ni/Pd/Au deposit which can prevent the Ni diffusion into Au instead of using just Ni/Au metallization. The embrittlement of the membrane was associated with the growth of a thin film of silicon dioxide on the surface and interaction with the gaseous species involved in the reaction which is different from fatigue-based failures in polycrystalline Si thin films. This failure mechanism is different from the normal fatigue failure of polycrystalline silicon thin film. The authors also suggested that further investigation is required to study the membrane embrittlement mechanism.

Hannigan et al. [121] investigated the studied corrosion products of four lead-free PWB finishes, OSP, ENIG, ImSn, and ImAg, generated in an MFG environment as shown in Fig. 10. The results showed severe corrosion on OSP, ENIG, and ImAg surface finishes, and minor corrosion, mainly due to oxidation, on ImSn surface finish. Similar corrosion products were observed on the OSP samples when compared to bare copper and their

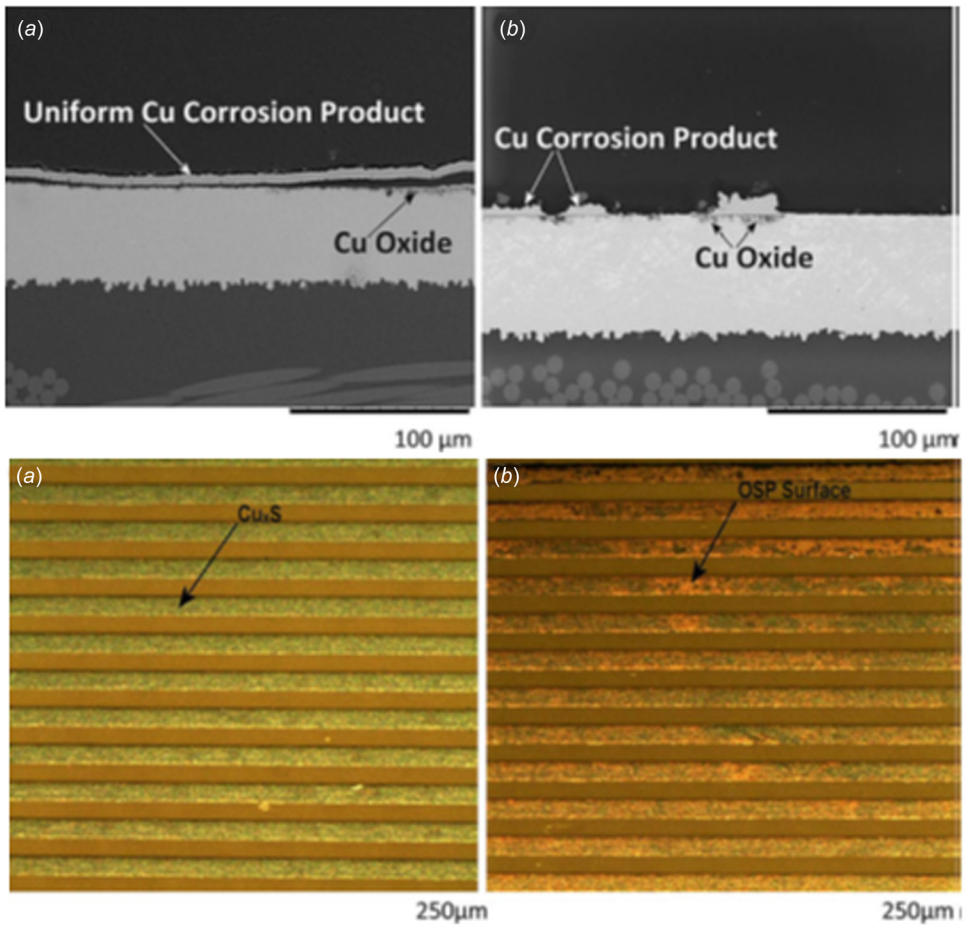

Fig. 10 (Top) cross section images of thin OSP and thick OSP after 15 days of MFG exposure and (bottom) stereomicrographs of adjacent leads of thin OSP and thick OSP after 15 days of MFG exposure

formation was mainly attributed due to the direct interaction of copper traces and corrosive gases. For the ENIG surface finish, the corrosion occurred mainly through the film porosity. The corrosion was found to be aggravated by the galvanic potential between gold and copper similar to the observations from ImAg [122–124]. Finally, excellent corrosion resistance was observed in the ImSn surface finish because of its inherent corrosion resistance in the MFG environment as well as the opposite galvanic potential between tin and copper compared with gold or silver and copper.

An important conclusion drawn from these studies is that temperature has a significant impact on ImAg surface finish than RH. Also, out of all the surface finishes and gaseous contaminants discussed ImAg appears to be more severely and easily corroded in presence of H_2S even for low RH values between 30 and 40 °C. Therefore, surface finishes such as ENIG, OSP, and ImSn should be preferred for data centers that are located in polluted geographies with high annual RH and temperature values and utilize airside economization or free-air cooling.

4.2 Flowers of Sulfur (FoS). The flowers of the sulfur test (ASTM-B809) is a corrosion test method published by the American Society for Testing and Materials (ASTM) to be used in pass/fail porosity testing of metallic coatings that are susceptible to corrosion in a sulfur environment [125]. The testing involves placing the test samples in a sealed glass chamber in a suspended manner with elemental sulfur and a potassium nitrate salt solution saturated with de-ionized water below the samples [126] as shown in the schematic in Fig. 11. This setup is then kept in an oven heated to a temperature of 50 °C causing solid sulfur to release vapors within the chamber. The saturated salt solution reaches a calculated amount of humidity in the chamber as it is heated at a fixed temperature for 24 h as narrated in the ASTM-B809 standard.

The literature points to the increasing use of FoS testing for surface finishes. This test method has also expanded for the evaluation of conformal coatings [127,128]. While the MFG test can sufficiently replicate surface finish failure rates, it has failed to do so in distinguishing the corrosion resistance level of surface mount thick chip resistors. The FoS technology, thus, has gained a

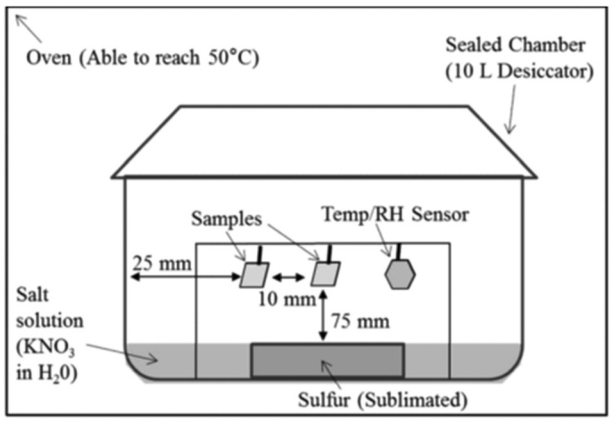

Fig. 11 A schematic of flowers of the sulfur test setup

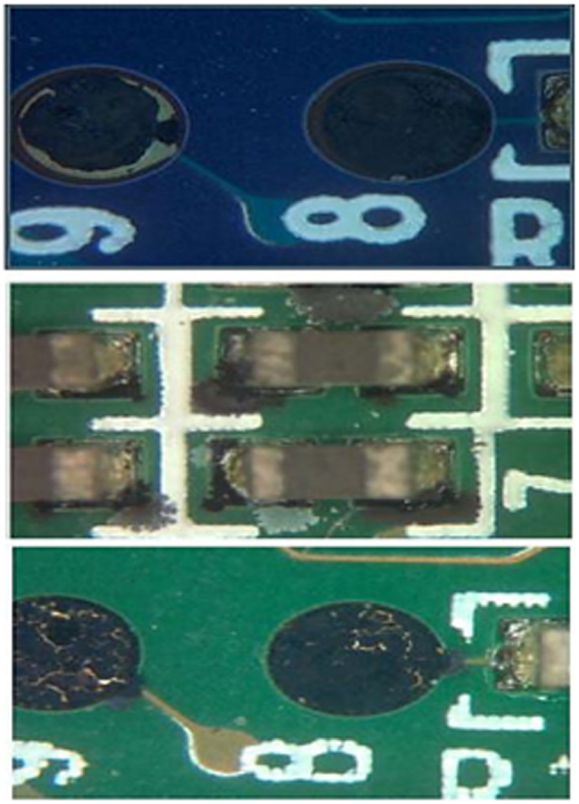

Fig. 12 Results of exposure of the PCBAs with the three finishes exposed to five days of MFG environment followed by exposure to FoS environment without Clorox™ for ten days and then to FoS environment with Clorox™ for 12 days

significant interest to establish the susceptibility chip resistors to corrosion due to attack from atmospheric sulfur in inner electrodes leading to failure [129].

Several studies by IBM (Armonk, NY) on modified FoS for creep corrosion measurement were reviewed. A 105 °C FoS test was successful for the qualification of miniature surface-mount resistors. An FoS test was also developed by an iNEMI subcommittee to test for creep corrosion on PCBs [130–134]. The low cost and the ease of control of the test variables were the main motivation for developing the FoS-based creep corrosion qualification test. The test conditions were:

(1) The test PCBs are baked in flowing nitrogen gas at 100 °C for 24 h.
(2) The relative humidity is maintained in the chamber using two 80 mm diameter Petri dishes filled with KCl saturated solution.
(3) The sulfur concentration is maintained using flowers of sulfur bed in two 100 mm diameter Petri dishes or in a 300 × 300 mm tray and by maintaining the chamber temperature at 50 °C.
(4) Chlorine is provided using 40 ml household bleach containing 6.25% sodium hypochlorite in a 100 ml beaker.
(5) Eight test PCBs can be mounted on the paddlewheel setup that is rotated at 20 RPM to circulate the air in the chamber and have some airflow over the test PCBs.
(6) The test duration of ten days is adequate. Susceptible PCBs suffer creep corrosion within five days.
(7) Any spread of the corrosion product over the test PCBs is an indication of creep corrosion.

A comparison between MFG and FoS study [135] was conducted for testing various PCB finishes like OSP, ImAg, and ENIG. The exposure times were 5–20 days in the MFG test and 12 days in the FoS test. The time for each test was chosen based on the acceleration factor sufficient to replicate the exposure of the PCBs for a time of one year in the field environment. The results for both experiments are shown in Fig. 12 and Table 6. In the MFG test, the ENIG PCBs suffered the most creep corrosion followed by the ImAg PCBs, with the OSP PCBs suffering the least amount of creep corrosion. In the FoS testing, the ENIG PCBs were the only ones that suffered significant creep corrosion, with the only slight extent of creep corrosion observed on the ImAg finished PCBs. In the FoS test, chlorine gas was confirmed to be necessary for creep corrosion. The morphology of the creep corrosion on the ENIG PCBs tested in the FoS chamber more closely resembled that observed in the field, compared to the creep corrosion morphology generated in the MFG chamber.

A study [136] to validate the iNEMI FoS technique was used to measure the corrosion rate of seven fully populated PCBs of various technologies and vintages of known field reliability histories. The silver corrosion rates during the FoS testing were measured by exposing a silver foil mounted on a rotating paddle wheel and measuring the thickness of the corrosion product using the coulometric reduction method. The silver corrosion rate was also measured using the electrical resistivity method on stationary silver thin films. Following were the results obtained from the study:

(1) Seven fully populated PCBs, from seven-part numbers, that were not baked were subjected to the iNEMI creep corrosion FoS test described above. The test duration was five days. Of the seven PCBs tested, only two PCBs (# 5 and #9) suffered minor creep corrosion; the rest did not suffer any creep corrosion. (2) The FoS test was repeated on seven fully populated PCBs from the same seven PCB part numbers, but this time the PCBs were prebaked at 100 °C in flowing nitrogen gas for 24 h to flush out the volatiles from the PCBs.

The test duration was 6 days. Of the seven PCBs tested, five suffered moderate to heavy creep corrosion in agreement with the field experience on these families of PCBs. The study demonstrated the validity of the iNEMI FoS technique and confirmed the necessity of prebaking the test PCBs in flowing nitrogen gas at 100 °C for 24 h. The creep corrosion occurrences on the PCBs agreed with field experience on PCBs from the same group as those tested and the results of the creep corrosion tests are as tabulated in Table 7.

4.3 Corrosion Classification Coupon and Reactivity Monitoring. Reactivity monitoring is a convenient and quantitative method to determine the corrosive potential of an environment by measuring the total corrosion film thickness on specially prepared copper coupons. Some studies [137,138] using "laboratory and field–exposed coupons have shown that using copper coupons alone can significantly under or overstate this corrosive potential". This method exposes coupons to the environment for 30 days and the resulting corrosion product thickness is evaluated by using coulometric reduction and chemistry. Using copper coupons alone has its limitation because of its inability to determine accurately

Table 6 Performance of the PCBAs in the MFG test [135]

Sn	Material	Days	Test results	Sn	Material	Days	Test results	Sn	Material	Days	Test results
FG00 6AV9	OSP	5	PASS	FOCO 85FA	ENIG	5	ISSUE	FOCO 85FS	ImAg	5	PASS
FG006 AM4	OSP	10	PASS	FOCO 85FB	ENIG	10	PASS	FOCO 85FM	ImAg	10	PASS
FG006 AZW	OSP	15	ISSUE	FOCO 85FH	ENIG	15	ISSUE	FOCO 85FW	ImAg	15	ISSUE
FG00 6AQ3	OSP	20	ISSUE	FOCO 85FE	ENIG	20	ISSUE	FOCO 85FX	ImAg	20	ISSUE

Table 7 Summary of the FoS creep corrosion test with and without prebaking (*x*-, *y*-, and *z*-represent hidden part number) [136]

Test PCB #	ID	PCB part number	Prebake	Corrosion results
1	2.5 DV1_10	xxxxx SPF	No	No creep corrosion
2	2.5 DV1_11	xxxxx SPF	Yes	No creep corrosion
3	2.5 DV1_20	xxxxx OSP Rosin	No	No creep corrosion
4	2.5 DV1_21	xxxxx OSP Rosin	Yes	No or minor creep corrosion
5	2.5 DV2_01	xxxxx SCI	No	Minor creep corrosion
6	2.5 DV2_02	xxxxx SCI	Yes	Heavy creep corrosion
7	3.5 DV1_01	yyyyy SCI	No	No creep corrosion
8	3.5 DV1_02	yyyyy SCI	Yes	Moderate creep corrosion
9	3.5 DV2_01	zzzzz SCI	No	Minor creep corrosion
10	3.5 DV2_02	zzzzz SCI	Yes	Heavy creep corrosion
11	3.5 DV3_10	xyxyx SPF	No	No creep corrosion
12	3.5 DV3_11	xyxyx SPF	Yes	Low creep corrosion
13	3.5 DV3_20	xyxyx OM	No	No creep corrosion
14	3.5 DV3_21	xyxyx OM	Yes	Heavy creep corrosion

the presence or absence of chlorine. On the other hand, using Silver alone also has its limitation when used alone because it is more sensitive to Chlorine. Therefore, it is important to use corrosion classification coupons using both copper and silver for accurate results for environmental classifications [138]. The use of Combination Corrosion Classification (CCC) coupons as adopted in these experiments using both Copper and Silver was then proposed as the most accurate classification of an environment. Sections 4.3.1 and 4.3.2 describe a set of laboratory-based and in-situ studies to classify a data center using CCC testing.

4.3.1 Laboratory Test. In this study corrosion classification coupons and corrosion sensors were both exposed to the same environment to compare results under the same conditions. To evaluate the predictive corrosion rate, an experimental set-up is developed with a corrosion classification coupon and sets of measurement and management technologies (MMT) corrosion sensors. MMT [139,140] is an integrated sensor for monitoring and capturing environmental data in data centers. To create an environment with a known contaminant (i.e., sulfur dioxide), a sulfur vapor concentration was created using FoS with the use of two reactants. The first reactant was pure sulfur flakes, and the second reactant was potassium nitrate, diluted in distilled water. The vapor cloud was continuously maintained within the test chamber that placed inside an environmental chamber while maintaining the temperature via the heater and the environmental chamber. After 72 h of exposure and readings were taken every 30 minutes, the result from the MMT sensors for corrosion, temperature, and relative humidity, results were obtained in the form of voltages which were converted to their respective values by using IBMs patented conversion table. Throughout the exposure time, a total of 648 Å and 502Å for silver and copper corrosion products, respectively, were estimated to have been deposited. This was deposited from a gradual temperature increase from room temperature 28 °C to a maximum of about 45 °C from the heater maintained at about 50 °C. From the copper and silver coupon, the corrosion products formed were copper oxides (CuO and Cu_2O), copper sulfide (Cu_2S), and silver sulfides (Ag_2S). The total corrosion film thickness measured for copper corrosion was 658 Å and for silver corrosion is 648 Å. These are above the G1 severity level and fall in the G2 severity level. The coulometric for both corrosion products were in solutions of potassium chloride (KCI) and none on the silver film. These results show the sensitivity of copper to oxygen as compared to silver. The result plots for both copper and silver coupons are shown in Fig. 13.

4.3.2 Combination Corrosion Classification in a Data Center. As an extension of the preceding study, a similar investigation was conducted at a real data center located in the more polluted geography of the Dallas industrial area. The data center considered in this study utilized a direct and indirect evaporative cooling unit. The location of the corrosion coupons was chosen as per ASHRAE requirements at 1/4 and 3/4 heights in front of the rack. The motivation behind the investigation was to provide a basis for ITE manufacturers to provide a warranty for their products in a G2 environment. The modular data center shown in Fig. 14 shows various sections of the research data center used for the field study of reactivity monitoring using the corrosion classification coupon technique [140]. The facility comprises a cooling unit, cold air supply ducts, hot air exhaust/return duct, IT pod, and I/DEC cooling unit. The 10 ft × 12 ft × 28 ft IT pod consists of eight racks with 120 servers, PDUs, UPSs, 120 storage devices.

The data center was equipped with MERV 11 to filter continuously particulates from the outside air. To classify the environmental condition of the location of the experimental data center coupons were placed at height locations 1/4 and 3/4 of the rack height as specified in ASHRAE guidelines to conduct such tests. For this testing, the coupons were placed facing the incoming air into the rack. At the locations shown in Fig. 15 below the coupons were left for 30 days after which the coupons were removed for coulometric/cathodic evaluation.

From copper coupon 1, placed at 1/4 of the rack height, copper oxides (*CuO* and *Cu_2O*) and copper sulfides (Cu_2S) were obtained as corrosion products. The total film thickness measured for copper corrosion was 102 Å at this location which is within the G1 severity level. As shown in Table 8, no copper sulfide (Cu_2S) was formed with the corrosion product for copper coupon 2, placed at 3/4 of the rack height. The total film thickness measured for copper corrosion was 122 Å at this location which was within the G1 severity level.

From the above results and observations, the silver coupons showed the highest corrosion thickness during the entire exposure at both locations. In the coulometric/cathodic reduction, the current densities used were 0.05 mA for all the coupons. It was also seen that there was no copper sulfide on the corrosion thickness for both coupons. In the laboratory experiment with the sulfur environment, copper sulfide accounted for the highest corrosion thickness. On the other hand, as seen from the results only silver sulfide was formed in both locations. In classifying this environment, the highest values of corrosion thickness were shown found out to be 373 Å at 1/4 rack height similarly 273 Å at 3/4 rack height which suggests that the data center could be classified as operating in a G2 environment.

5 Computational Studies on Gaseous Contamination

Computational fluid dynamics (CFD) proves to be a valuable tool in reducing the gap between purely analytical and experimental work using well-established laws of flow and heat transfer. Provided, accurate numerical setup, CFD is usually fast and well precise in replicating near similar results as obtained from experiments inexpensively. While there is a large number of studies related to the thermal evaluation of data centers, CFD has not

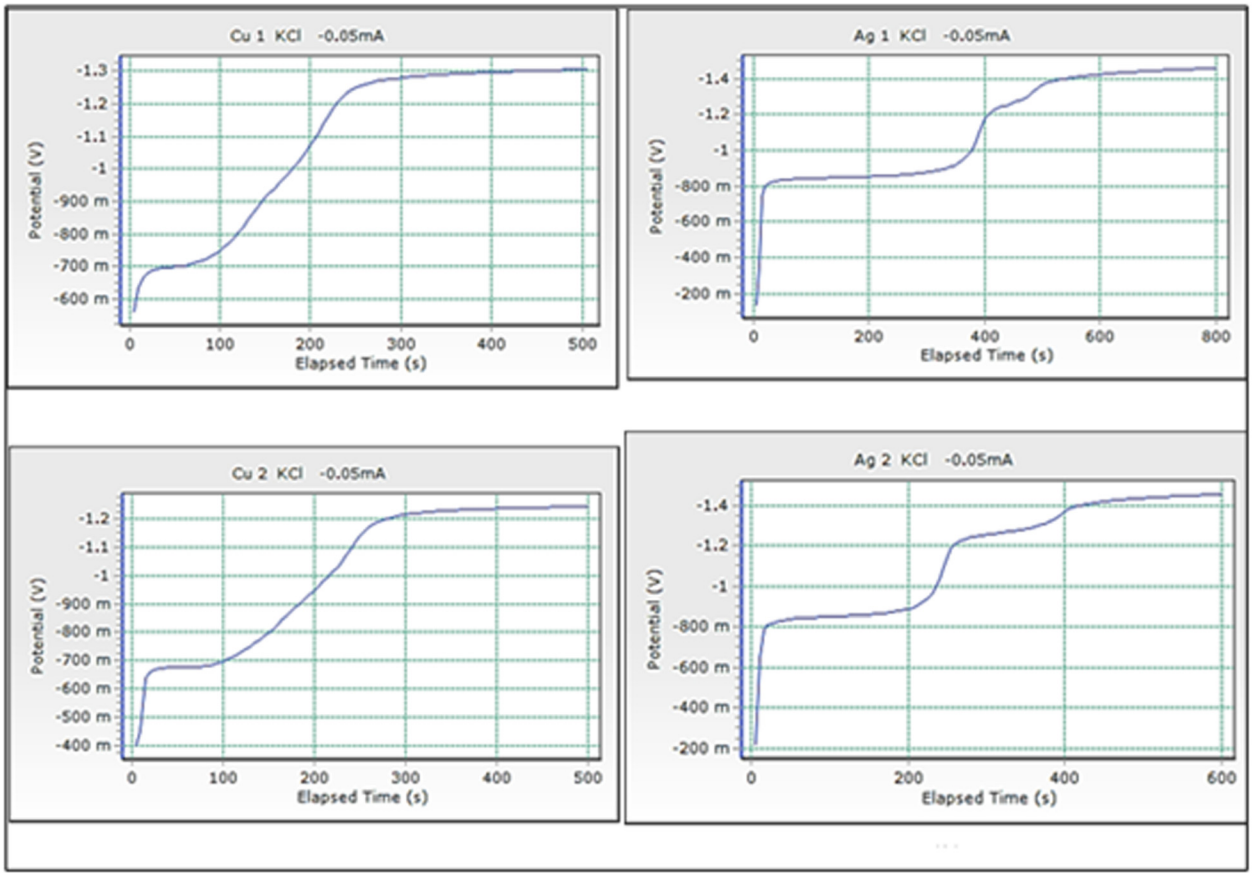

Fig. 13 The plot of coulometric/cathodic reduction for copper (left) and silver coupons (right)

been as widely used for reliability assessment. Sections 5.1 and 5.2, review some of the important research works that utilize CFD for predicting corrosion rates for electronic equipment due to gaseous contamination.

5.1 Gaseous Contamination in Hard Disk Drive. Hard disk drive (HDD) is the largest data storage device. A hard disk drive stores digitally encoded data. In 1956 IBM introduced the first HDD to store digital data [141]. A typical HDD consists of a casing, an actuator arm, actuator axis, head, spindle, platters, power connectors, and packages on flexible substrates. The motherboard is connected to the back of the hard drive through the port of cable provided at the back end of the HDD. The performance of the HDD relies on the air pressure from the outside environment for maintaining a certain flying height while the platter is rotating. The pressure and contact with the environment are maintained by a small breather port. The breather port is the only place where the outside environment can encounter the internal part of the HDD [142].

When gaseous contaminants meet the platter after destroying the carbon film, the magnetic layer starts corroding as the co-based magnetic layer doesn't have mechanical durability and corrosion resistivity. Air enters the HDD through the breather port when the HDD is powered on. Contaminants encounter the parts of HDD using air as a medium [143]. According to the study carried out by Waltman and Khurshudov, by using atomic force microscopy for a seven-day test, when a slider meets the disk surface, mechanical wear takes place on both the disk and slider surfaces. Literature suggests that the 40 Å carbon film on the slider can be worn away within 2 days due to the wear rate decreasing significantly thereafter and the contact surface of the slider loses the protective carbon film as well [143]. According to the study, the number of spots of corrosion is seen less with increasing the thickness of the lubricant layer. The number of spots of corrosion increases when the thickness of carbon film reduces from ~50 Å.

For the computational study on simulating corrosion on HDD, a simplified three-dimensional model of main components was developed [144]. The geometry included a rotating disk, and spindle, and an actuator arm mounted on the actuator axis along with the magnetic head mounted on the actuator arm. For the reviewed study, the mixture materials were defined along with the properties of the materials involved in the chemical reaction which was

$$CoO + H_2O + SO_2 \cos O_4 + H_2 \quad (1)$$

For the simulation, H_2, H_2O, and SO_2 were defined as the gas-phase species, CoO was defined as the site species and $CoSO_4$ is defined as a solid species. For determining the rate of deposition of sulfate on the rotating platter two different cases were employed, wherein case 1, the relative humidity (RH) was varied, and in case 2, the rotational speed of the platter was varied to study the effect of change in humidity and change in rotational speed of the platter on the deposition rate of sulfate on the platter. For investigating case 1 the RH was varied from 30%, 40%, 50%, 60%, and 70%. The rotational speed of the platter, in this case, was kept constant at 7200 RPM. The inlet temperature was held at 301.15 K and the operational temperature was kept constant to 328.15 K. For investigating case 2 the rotational speed of the platter was varied from 5400 to 14,000 RPM with a constant RH of 50%. The inlet temperature was kept constant to 301.15 K and the operational temperature was kept constant to 328.15 K. The results of the deposition rate with varying RH% and RPM are given in Fig. 16. The study concludes that increasing the RH harmed sulfate deposition and there was no significant effect of increasing RPM on the deposition rate on the HDD platter.

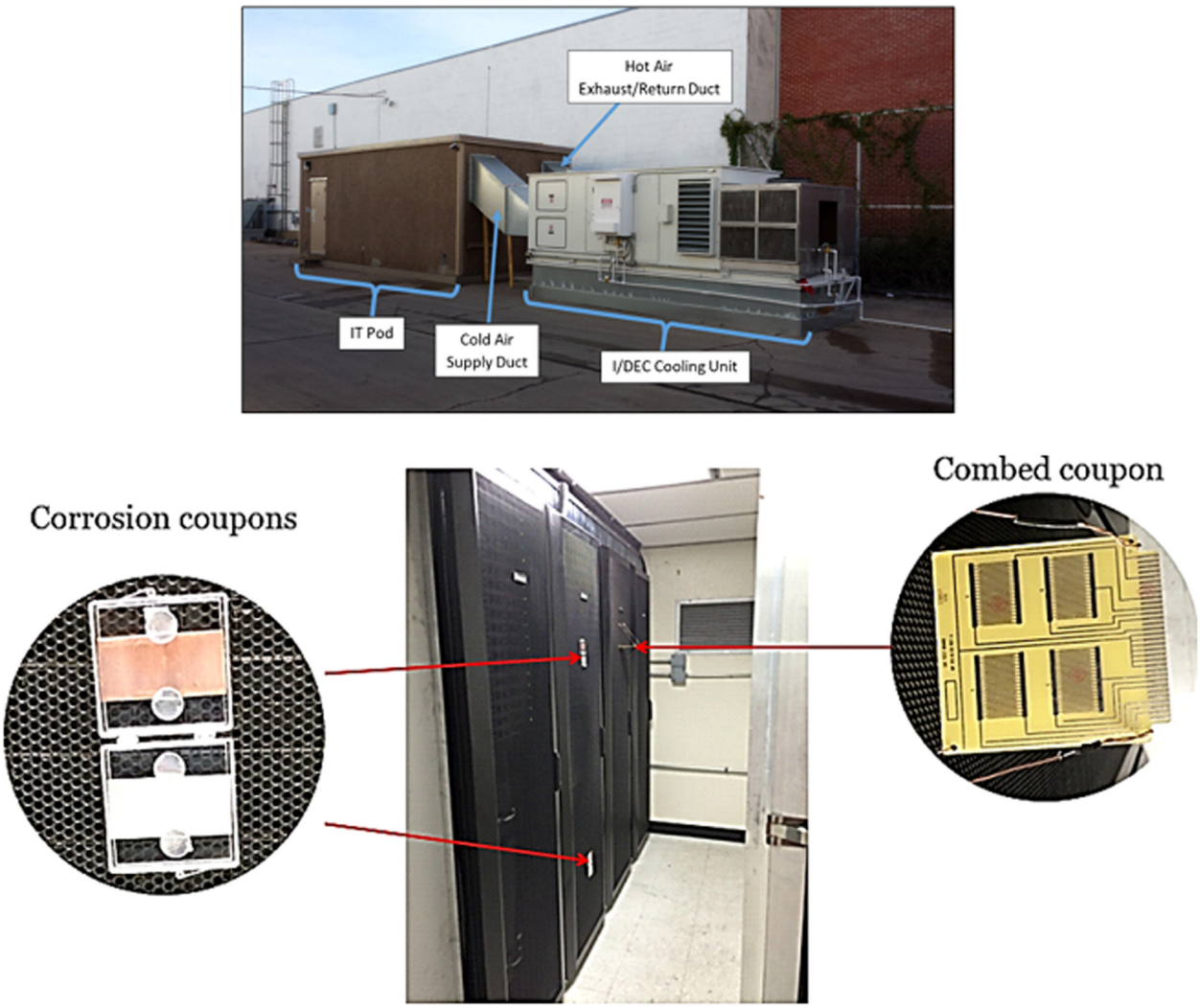

Fig. 14 Research modular data center (top), copper, silver, and PCB comb coupon locations inside the IT pod (bottom)

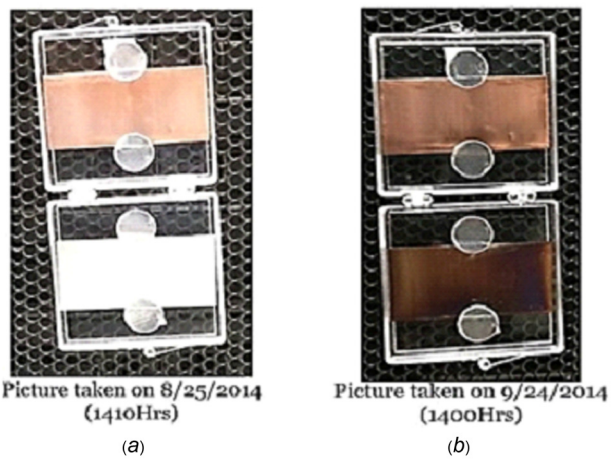

Fig. 15 Copper and silver coupons before (left) and after exposure (right) for 30 days in the field data center

5.2 Computational Study of Gas Absorption in Information Technology Equipment. To study the effects of contamination in real-life data centers can be a tedious task, therefore, computational studies save a lot of time and cost in such scenarios [145]. As discussed in Sec. 4.2, FoS can provide a simpler and cost-effective way of determining the ITE reliability in a corrosive environment by also considering the impact of air velocity using a rotating paddle wheel. The subsequent computational study describes the reaction mechanism of corrosion due to gaseous contamination, H_2S, and SO_2 with varying RH, using a paddle wheel test setup. In this investigation, the effect of various gases has been tested on ITE without using the actual equipment.

The geometry of the experimental setup was modeled in commercially available CAD software where the dimensions of the solid model were the same as that of the actual model. The Petri dishes, as present in the original test setup, were eliminated by using four inlets and outlets each on the top and bottom of the chamber during modeling. Velocity and species concentration (35 ppm of H_2S or SO_2) boundary conditions were given at these inlets with the humidity of inlet air between 10% and 60%, at steps of 10% increment, and a temperature between 292 K and 298 K at steps of 1 K. A 20 RPM rotating boundary condition was given to the rotating parts (carousals and foils) within the chamber about the central shaft.

A total of 54 simulations were conducted by the authors to monitor the effect of H_2S and SO_2 on the rate of corrosion. The results showed that there was a regular behavior observed in the corrosion rate in most of the cases with varying temperature and humidity for both the gases considered for the simulations. Although, there were some points in the simulation that did not follow the same trends as shown in Fig. 17. The overall results showed that the corrosion rate was less severe at the same

Table 8 Field results for corrosion coupons [140]

Coupon	Copper corrosion product	Seconds	Thickness of corrosion product (Å)	Exposure days	Copper corrosion rate (Å/month)
1	Cu_2O	98	68		102
	CuO	94	34	30	
	Cu_2S	0			
2	Cu_2O	133	92		122
	CuO	83	30	30	
	Cu_2S	0	0		

Coupon	Silver corrosion product	Seconds	Thickness of corrosion product (Å)	Exposure days	Silver corrosion rate (Å/month)
1	Ag_2S	373	363	30	363
2	Ag_2S	240	233	30	233

thermodynamic conditions for SO_2 than H_2S. Although the results of this study were not validated against experimental results, the study proposes a good approach. If a calibrated CFD model can be developed using experimental results, the CFD model can then be used to vary different environmental parameters without having to run different experimental cases.

6 Experimental Studies on Particulate Contamination

As discussed earlier, data centers use a huge amount of energy to cool down the computing and power distribution equipment. Airside economization has been one of the measures that data center administrators are choosing to control the rising cooling costs. A threat that the ITE suffers when the relative humidity and temperature is not mechanically controlled is of introducing particulate contaminants in the white space along with the free cold air. Information and communication companies, including companies like Google, Microsoft, AWS, and Facebook have adopted airside economization methods as a means of reducing greenhouse gas emissions and energy costs [146,147]. Section 6 will review studies related to reliability issues caused by settled hygroscopic matter on ITE, particularly in data centers utilizing free air cooling. These studies also propose possible solutions in estimating the operating RH of data centers utilizing free air cooling and characterizing the settled contaminants to expand the ASHRAE envelope. Section 6 will also provide a brief overview of the Airside Economization and the effects of relative humidity on ITE.

The first study reviewed in Sec. 6.1 aims at conducting a qualitative analysis of cumulative corrosion damage of ITE for a modular data center with a measured ISA air corrosivity level of G2. The second is based on identifying and characterizing the morphology of the particulate contaminants found inside the same data center. The third study proposes and validates a cost-effective methodology to determine the DRH of pure salts like magnesium chloride ($MgCl_2$), ammonium nitrate (NH_4NO_3), and sodium chloride (NaCl) using a well-tested experimental process for DRH characterization of ionic matter. These values were then corroborated with existing published literature. Finally, the methodology for DRH characterization of pure salts was used to determine the DRH of different samples of dust taken from actual servers in the field.

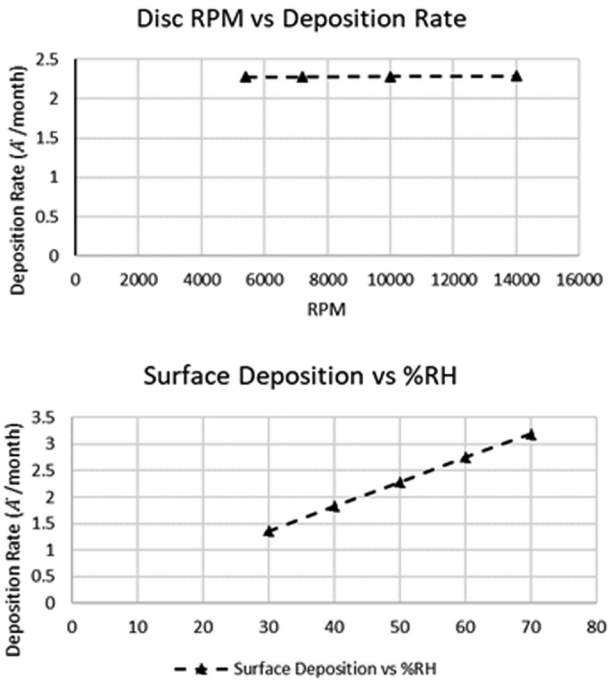

Fig. 16 (Top) Rate of deposition of sulfate on the platter with varying RPM and (bottom) relative humidity

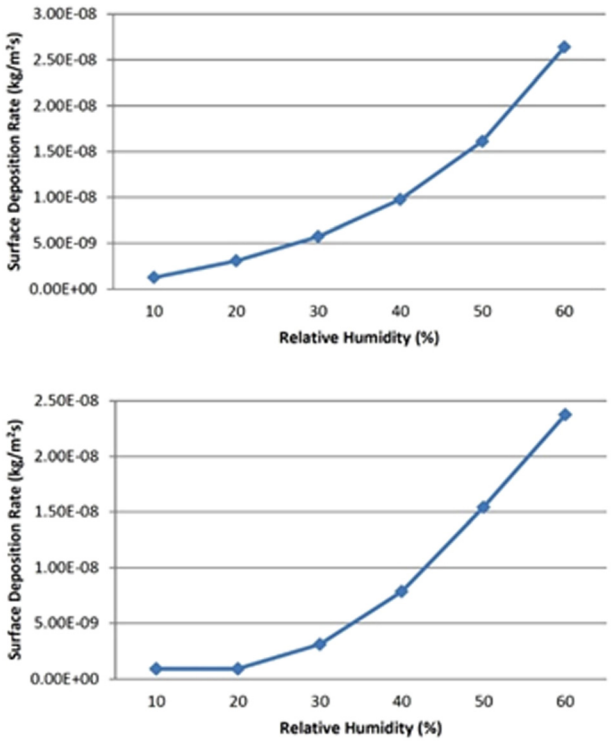

Fig. 17 (Top) Surface deposition rate at 300K for H_2S with varying RH (top) and SO_2 (bottom)

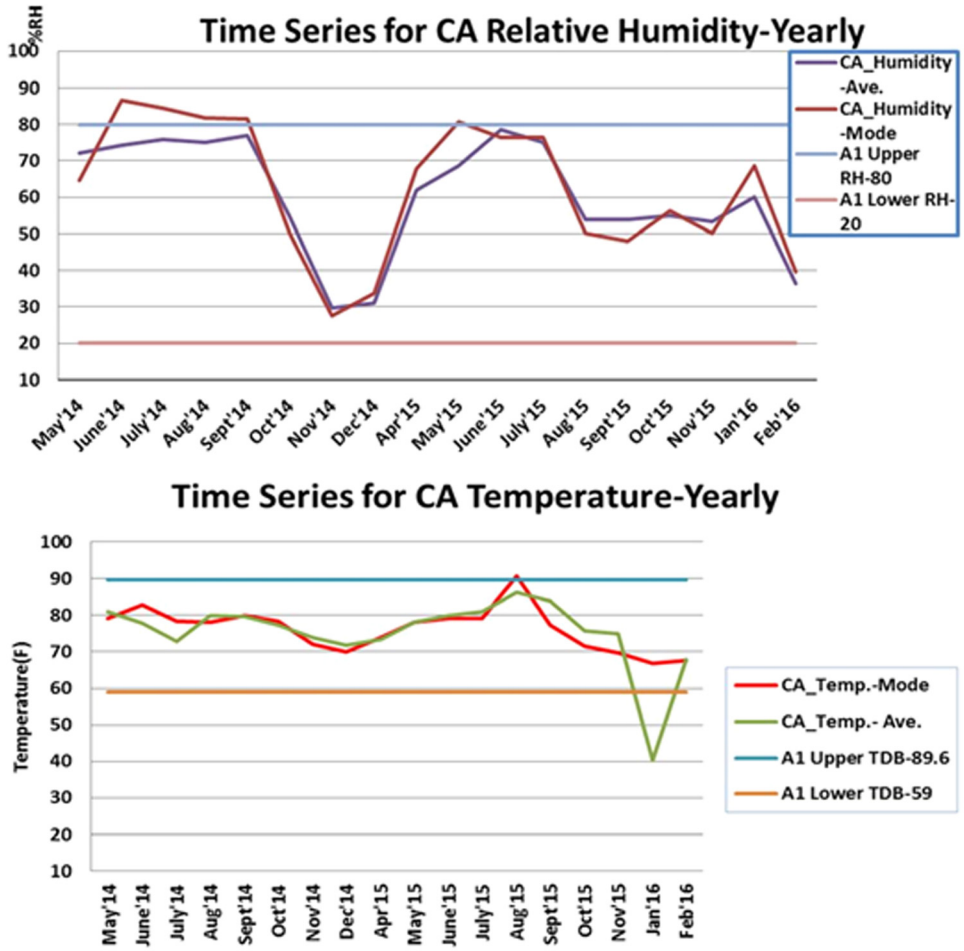

Fig. 18 Average variation of (top) yearly humidity and (bottom) yearly temperature at the modular data center site

6.1 Qualitative Analysis of Corrosion. This study addressed the hardware reliability issues for a research modular data center located in an environment with corrosive potential severity levels between G2 as per ANSI/ISA 71.04 [148]. This modular facility used an Indirect/Direct Evaporative Cooling unit for cooling the IT hardware. A qualitative assessment of the corrosion damage was carried out by comparing the physical state of the server and its components before and after installation in the IT Pod. For a baseline comparison of the qualitative results, the results of visual inspections were compared with a visual inspection of the same servers stored in a laboratory data center. The laboratory data center is cooled by a 20-ton CRAH unit with a surrounding environment assumed to be compliant as per ANSI/ISA 71.04 G1 corrosion severity potential. The laboratory data center is maintained at a constant 18 °C supply temperature. Daily statistical analysis for the average %RH and temperature values at the modular data center site were conducted. The results showed that over two years, the site operated in ASHRAE A1 allowable envelope for the maximum time of operation. The cold aisle dry bulb temperature varied between 15 °C and 32 °C. The yearly variation of both temperature and humidity at this site is shown in Fig. 18.

For qualitative assessment, visual inspections of the parts internal to the server chassis like flow hoods, chassis cover, motherboard, and heat sink were conducted as seen in Fig. 19. The images represented by NH were taken from an idle server located in the cleaner, laboratory data center. A significant amount of particles were found on the inside of the chassis cover of the servers inspected at the modular data center site. Images of the server motherboard show onset of corrosion on copper parts as seen in the top part of Fig. 19 in MH#1 and MH#2 (two different servers). The implications of these inspections can be an electrical failure if the DRH value of the dust mixture found in the servers is less than 80%. The lodging of dust inside the heat sinks can degrade both the thermal performance and increase server pressure drops due to increased fan RPM. Dust with thermally insulating properties can also lead to component overheating. Clogging and dust deposition on fan blades can deteriorate fan performance and change system-level acoustics.

6.2 Identification and Characterization of Contaminants. In this subsequent research, a few servers were randomly removed from the racks and a qualitative study of cumulative corrosion damage was carried out [149,150]. The particulate matter was characterized using scanning electron microscopy (SEM), energy dispersive spectrometer (EDS), and Fourier transform infrared spectroscopy (FTIR) as shown in Fig. 20. The figure at the top depicts the particle sizes measured at random locations using image analysis in MATLAB. As seen the maximum and minimum particle sizes of approximately 50 nm and 24 nm, respectively, depict that ultrafine particle matter is capable of escaping through MERV 13 filters in the data center white space based on filter removal efficiency. The data analysis of the obtained particulate matter showed that Carbon was the most pervasive element found in the collected sample and an average particle size of 11.03 ± 2.09 nm. It can be inferred that most of the particles are small enough to pass through the filters used in most of the data centers.

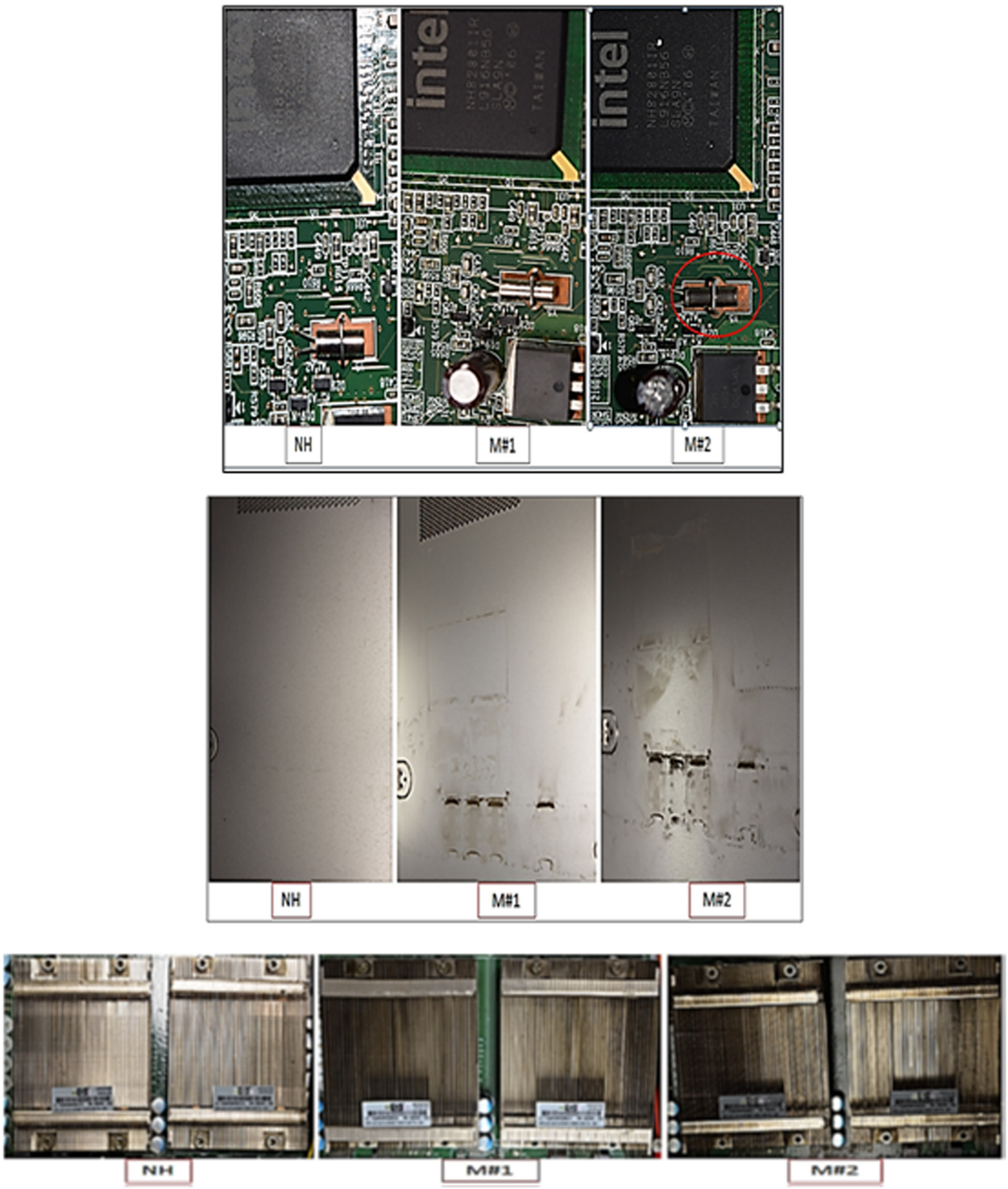

Fig. 19 Images taken at the laboratory data center and the modular data center site showing (top) dust accumulated on PCB and copper (middle) fine dust particles lodged above server flow hood and fan shroud (bottom) dust accumulated between heat sink fins

6.3 Determining the Operating Relative Humidity for a Real Data Center. The primary objective of this research study was to develop a set of experiments that can accurately measure the DRH value of the particulate matter, cost-effectively, found in data centers [151]. To accomplish this, the electrical impedance method was used to first determine the DRH of pure salts and validate the methodology by comparing the results obtained with the standard DRH value of these salts in the literature. The salts considered in this study were sodium chloride (NaCl), ammonium nitrate (NH_4NO_3), magnesium chloride ($MgCl_2$). The published values of the DRH of the salts used in the study are 75.8% for sodium chloride, 64% for ammonium nitrate, and 32.78% for magnesium chloride. IPC-B-25A multipurpose test boards were used for comprehending the effect of moisture and insulation resistance of solder masks. The Arduino Uno and INA219 [152,153] current sensor arrangement was connected to the test

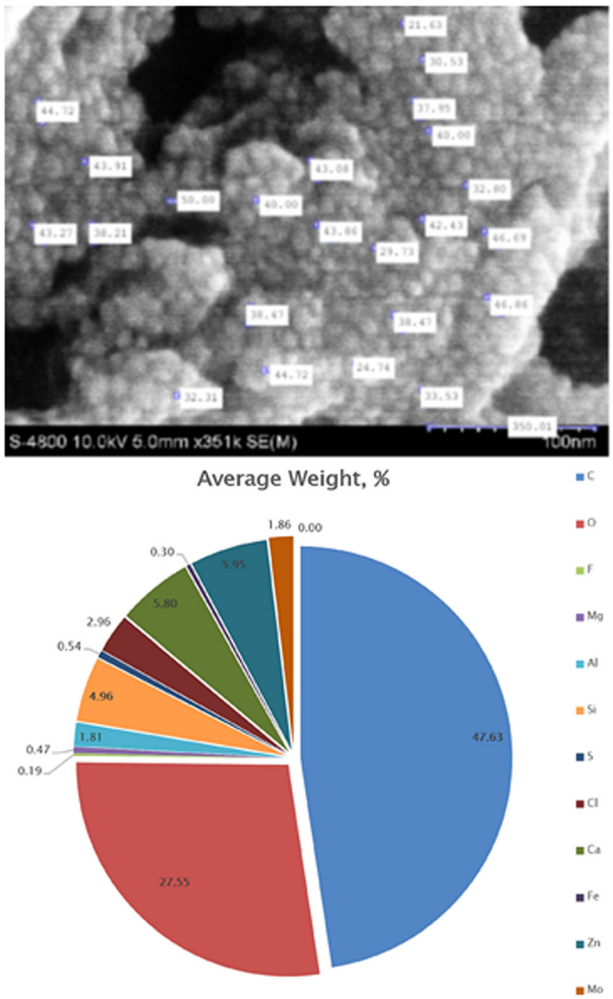

Fig. 20 (Top) size of the particulate matter (nm) and (bottom) the average weight of elements identified in the contaminant sample in percentage

board which was placed in an isothermal environmental chamber. To prepare the test sample, 10 mg of the salt was dissolved in 10 ml of de-ionized water thus resulting in the 0.1 wt% concentration. The salts, in the form of a slurry, were carefully dispensed on the test boards with the help of a sanitized suction syringe as shown in Fig. 21.

The experimental runs were carried out at a constant temperature of 25 °C with a 12 h rest period to get rid of the moisture from the solution. After the completion of the first cycle, a dc voltage of +1 volt was applied across the test board and the corresponding leakage current was recorded. After this, a voltage of −1 volt is passed through the coupon to neutralize the effect of the positive bias on the ions. The percentage of RH was increased by 10% until RH% of 90% was reached by repeating the steps for recording the readings. The obtained values of the logarithm of the leakage current and RH% are used to obtain the CRH and DRH of each salt sample as shown in Fig. 22 and the comparison of the results with the published literature is shown in Table 9. Since the results obtained from this study closely matched the values in published literature, it was ascertained that the same methodology can be used to find the DRH of dust or particulate matter found in data center ITE.

The subsequent study [152] by the authors was carried out for determining the operational RH for a real data center by determining the DRH of accumulated dust in the servers in a research modular data center. Four dust samples were collected from randomly picked serve chassis at various heights using de-ionized water.

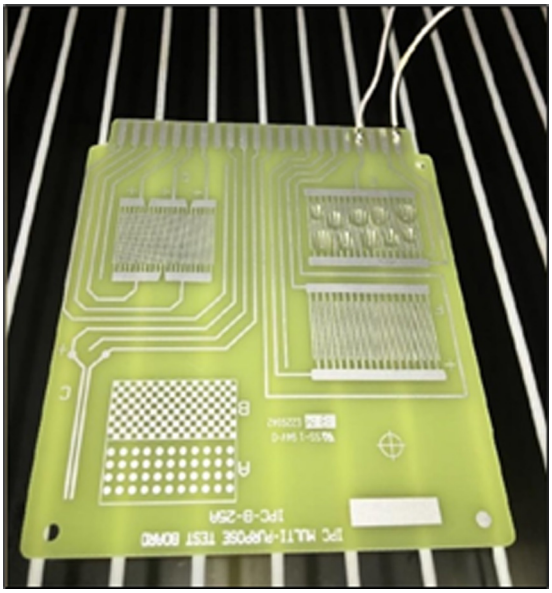

Fig. 21 Multipurpose test board used for the experiment with deposited contaminated salt slurry

Another sample of facility water, which is used in the D/IEC unit was also collected. After validating the approach for pure salts, the same procedure was used by the authors for obtaining the DRH for dust samples from the modular data center and is narrated and the results are shown in Fig. 23.

In both these studies, a cost-effective and precise methodology to establish the DRH of accumulated particulate matter is described. The logarithmic plots of the leakage current versus RH percentage depict the values of the CRH and the DRH of pure salts as well as dust samples. The authors claim that the entire setup is cost-effective, fast, reliable, and easy to handle. It is evident from the linear graphs of dust samples from a real data center that there is a sudden increase in the value of leakage current at %RH of 60% for server 1 showing that there is an increase in electrical conductivity on the test boards. For server 2, server 3, and server 4 and, facility water, the linear plot showed that the leakage current value increased suddenly at an RH% of 50% but had similar trends to server 1, so were not shown in the paper. As for the facility water, the linear graph showed that the experimental value of DRH is 80%. Based on this series of studies [148–152], it can be concluded that for the data center site studied in these investigations the DRH value of the particulate matter lies between 70 and 80%. Therefore, the operating relative humidity inside the IT pod of this site should be maintained below this range. A similar approach can be used for data centers, that wish to utilize indirect/direct evaporative cooling, to quantify the failure risk posed to ITE when operating outside the ASHRAE recommended temperature and humidity range.

7 Computational Studies on Particulate Contamination

Experimental studies, especially for system-level particle transport analysis are an expensive venture. High precision equipment like aerosol generators, particle counters, and high sensitivity leakage current detectors can ramp up the cost of such a setup to tens of thousands of dollars. In the past, computational analysis for particle and pathogen transport has been done for indoor environments, especially for commercial buildings and aircraft. These studies have been able to provide a first-hand idea of possible issues that can arise due to harmful airborne particle transport and assist in providing mitigation strategies from corresponding mechanical design changes. The following research investigations

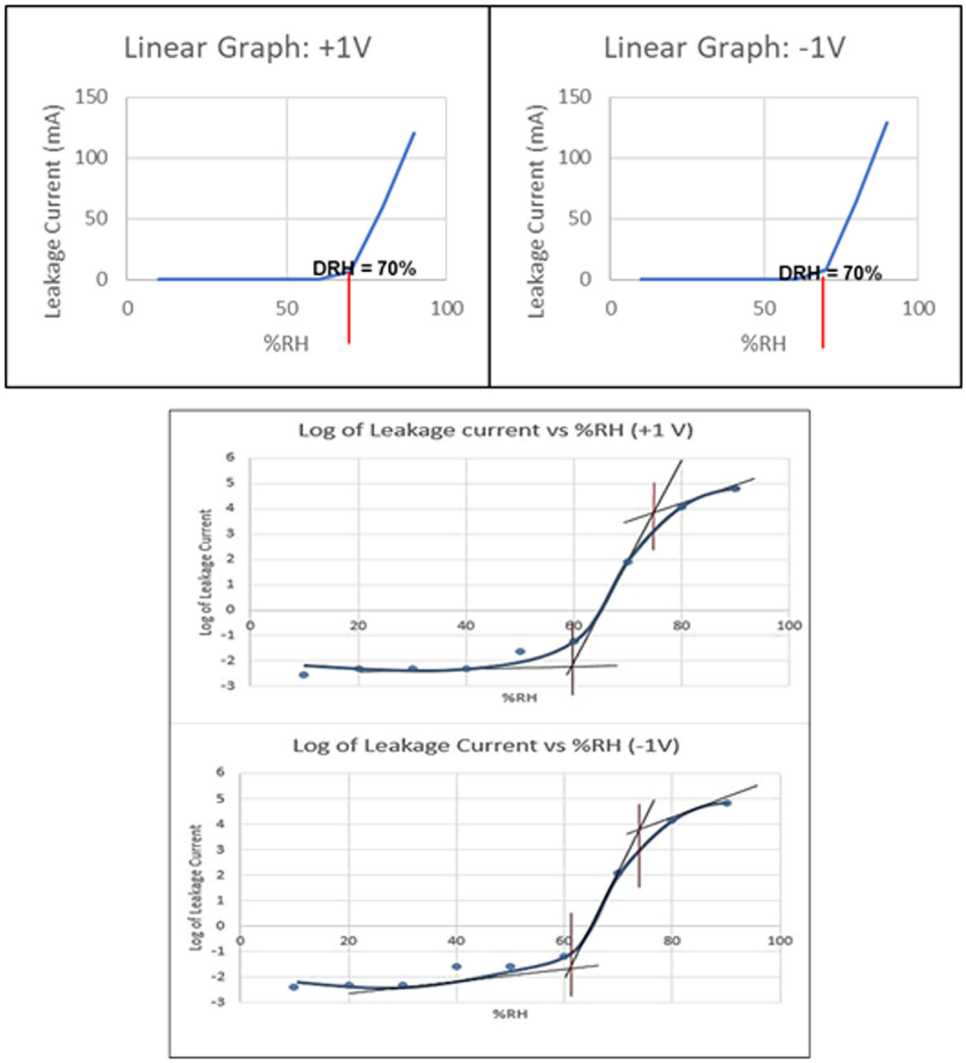

Fig. 22 (Top) linear plot of leakage current versus %RH for NaCl (+1 and −1 Volt) and (bottom) logarithmic plot of leakage current versus %RH for NaCl (+1 and −1 Volt) [151]

Table 9 Comparison of experimental results with the published results by analyzing the linear plots of leakage current versus %RH [151]

Salt	Published values at 25 °C	Experimental values (linear plots)
Sodium chloride	DRH: 75.8%	DRH: 70%
Ammonium nitrate	DRH:64%	DRH: 60%
Magnesium chloride	DRH: 32.78%	DRH: 30%

have been conducted in recently published literature, being motivated by particle transport in ventilated environments like medical operating rooms and confined ventilated spaces, for example, an aircraft cabin.

Computational fluid dynamics modeling is the process of representing a fluid flow problem by mathematical equations based on the fundamental laws of physics and solving those equations to predict the variation of velocity, pressure and temperature, and other variables such as turbulence parameters and concentrations which are discussed by Jones [154]. The study also describes that it is also possible to predict the spatially and temporally varying distribution of particulate contamination within the space and hence, evaluate ITE reliability. Two studies that closely relate to the type of particle transport model with the reviewed study were by Chen and Zhang [155] which evaluate the flow using Reynolds-averaged Navier–Stokes (RANS) and large eddy simulation. The other study by Seymour [156] used the Lagrangian approach, where the assumption that the volume fraction of particles is very less than that of total airflow and the particles do not influence the flow of air. computational fluid dynamics, when applied to airflow distribution within data centers have the potential to predict the velocity and temperature distributions. The research also concludes, that in any contamination control applications, the particles are of submicron level and at this size, there is little slip relative to the air in which they are situated. As a result, the particulates are considered as completely airborne and treated as if they are gaseous.

By using this as a base assumption, Thirunavakkarasu et al. [157] used the physical properties of air (molecular weight of 28.9 kg/mol and density equal to 1.19 kg/m^3) for 0.05 μm and 0.1 μm particles. The objective of this study was to deal only with the effect of the concentration of airborne contaminants on the

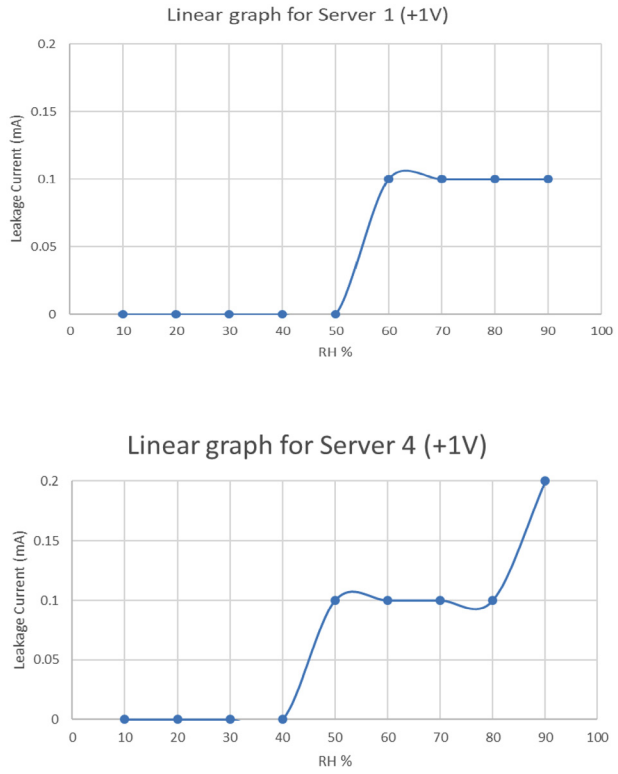

Fig. 23 Linear relation graphs for DRH of dust samples from server-1 (top) and server 4 (bottom)

wall surface of the servers at different rack heights in a cold aisle. The study assumed the air conditioning unit (ACU) as the source of contaminants to simulate free air-cooling during economizer hours. The contour plots and the streamline plots show the concentration of the contaminants in the room at a height of 1 meter off the raised floor. The number of particles per million (ppm) of the contaminants is chosen to be 10,000 particles for 0.05 μm and 0.1 μm and 900 particles for 1 μm, for a transient period of 10 minutes. Both the simulation results were run for a transient time duration of 10 minutes and during this time, the migration of the particulates is observed either as streamline trajectories or concentration plots. When examining the streamlined trajectories of the hot-aisle model, the maximum concentration is found to be around the first three cabinets on either side of the hot aisle. Similarly, for the cold-aisle model, the concentration plot reveals the maximum accumulation of particulates at the far end of the ACU, i.e., the last row in the first aisle of the model.

As the authors assumed, the particles of size 0.05 μm and 0.1 μm followed the same path as air since they have the same physical properties as air. The streamline plots obtained show the velocity vectors of the particles emanating from the ACU and entering the server racks which describes the flow pattern and path. The concentration plot, which is a plane at 1 m height in the room, shows the region of the most particle concentration. Figure 24 shows the comparison of the contaminant concentration on a result plane based on particle size. It can be concluded from the top part of Fig. 24 that the particle size of 1 micron shows a different concentration pattern than the one below where particle size is 0.05 micron at similar time intervals. The sensor plots for contamination percentage were also obtained by placing six sensors at 0.5 m height from the raised floor on three cabinets on either side of the hot aisle to describe the variation of contamination with increasing time at that height. It was also observed that the contamination level reduced with increasing height in both cold aisle containment and hot aisle containment.

In recent research done by the authors [158], particle transport was studied using CFD for a simplified model of a raised floor data center. A commercially available CFD code ANSYS FLUENT was used to simulate particle transport using a Lagrangian approach. As shown on top in Fig. 25, a rectangular flow domain was modeled with the bottom side depicting particle inlet through a floor tile. One of the other boundaries in the flow domain was given a low-pressure boundary condition, depicting the side facing the servers. It was concluded that particle size or particle mass is the dominant factor that dictates particle dispersion. The lighter or lower diameter particles in the flow domain showed a rather random dispersion pattern. The particle concentration plots, shown in Fig. 25, showed that particle deposition was more pronounced around the bottom servers due to low-pressure regions. The particle escape regions were inferred to be located toward the bottom of the flow domain, implying that the maximum particle concentration or deposition should be found in the servers located at the bottom of the flow domain. The results suggested that the total mass and the number of particles that escaped from the top outlet were approximately four times greater than the outlet facing the servers. For high-density particles, the total particle count injected in the flow domain was nearly 1.9×10^{11} and the fraction of particles escaping toward the servers was an order of magnitude more than that obtained for lighter particles.

8 Outlook

Based on the literature reviewed, future research needs to quantify the failure rates using in-situ studies for both particulates as well as gaseous contaminants. Conventional air-cooling technologies will continue to dominate the data center cooling industry. Therefore, efficient air-cooling technologies like airside economization using indirect/direct evaporative cooling will continue to play an important role in bringing down the power usage effectiveness and carbon footprints of the data centers. This will require a systematic effort to address the equipment reliability issues that thwart the data center managers from a successful implementation of these energy-efficient cooling technologies. Characterization of failure rates due to particulate and gaseous contamination for different regions in the ASHRAE recommended and allowable envelopes will provide a significant boost to this effort. This will allow the IT equipment manufacturers and data center administrators to directly co-relate the performance of the IT equipment with the ambient environment. Quantification in terms of degradation in the server's thermal performance, degradation of packaging material mechanical and electrical properties needs to be conducted. Ionic sensors and chemical gas phase filtration strategies should be mandatory for large-scale enterprise data centers that use free air cooling as a primary mode of cooling for a large portion of the year. Ultra-fine and fine particle categories that include ionic salts and volatile organic compounds are particularly harmful to data centers located in industrialized geographic locations. While it is easier to remove coarse particles from entering the data centers using MERV 8 to MERV 13 filters, they are not as efficient for ultrafine particles which may require filters of MERV 16 and above, especially those with low DRH [159–161]. An otherwise ignored parameter, wind direction can play a very important role in free air-cooled data center design and ITE reliability. An optimal design of air inlets per wind direction and away from backup generators prevented smoke entry into the data center in a fully free air-cooled open compute data center owned by Facebook [162]. Another major gap in the reviewed literature is the lack of data on failure case studies due to ionic dust. The same is still available in the form of case studies for failures due to corrosive gases [163]. Research work similar to that of building and cabin thermal comfort analysis using CFD can be done at the data center level for assessment of particle flow, regions of accumulation, and particle terminal velocities. This will require a synergistic effort from the data center managers, IT equipment OEMs, and academia.

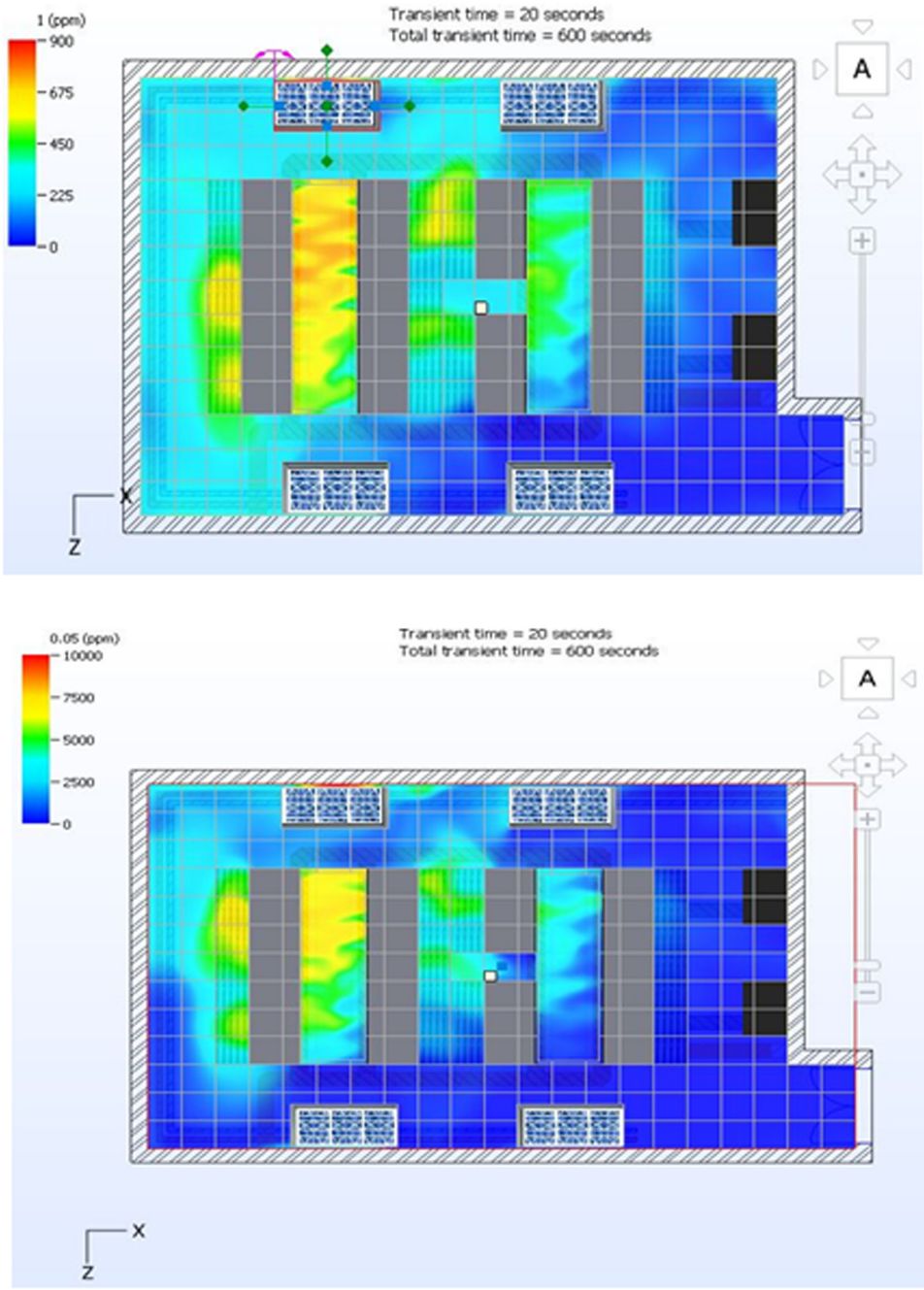

Fig. 24 Concentration plots showing particle distribution in a two-dimensional plane in the data center for the particle size of 1 (top) and 0.05 micron (bottom)

9 Conclusions

A critical review of degradation of ITE reliability in airside economized data centers due to gaseous and particulate contaminants was presented. The effects of airborne contaminants introduction inside the data center on the ITE reliability and associated failure modes such as creep corrosion, corrosion of silver terminations of surface mount components, and ECM are discussed in detail. A detailed account of the methods to determine the reliability of data center electronics in harsh gaseous environments and due to settled hygroscopic particulate contaminants is documented. It was observed that MFG is one of the more researched and widely used qualification techniques for testing PCBs for creep corrosion in a gaseous environment. But some recent studies point out the fact that FoS can be a cost-effective and more convenient approach to reproduce creep corrosion in the lab environment which more closely represents field results of ITE corrosion.

It is concluded that significant research needs to be conducted to develop correlations between the reliability degradation due to particulate contamination and the surround environment for airside economized data centers. As in the case of gaseous contamination, humidity and temperature x-factors also need to be quantified for particulate contamination as shown in Fig. 26 [164]. The primary challenge in establishing these values is the unpredictability of the failure mechanisms associated with particulate contamination. Also, it is difficult to produce similar failure rates using laboratory testing since the synergies between various gaseous pollutants and airborne particulates cannot be simulated in a lab environment. Real-time monitoring of data centers and

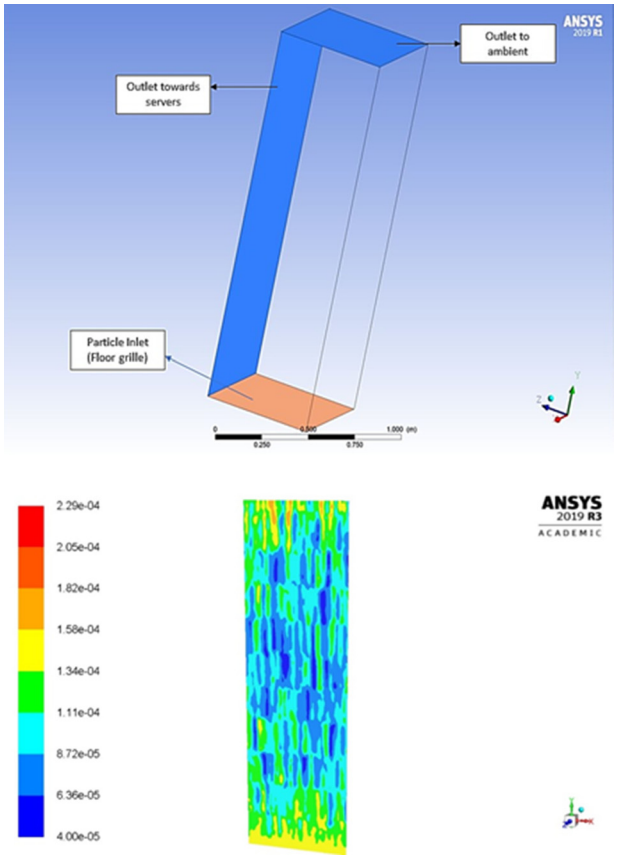

Fig. 25 (Top) boundary conditions used in the CFD study (bottom) particle diameter distribution at the side facing server inlets for high-density particles

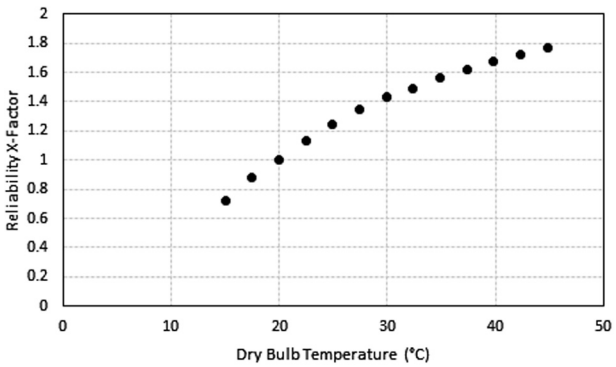

Fig. 26 IT equipment failure rate as a function of temperature

gathering historical environmental data and weather bin analysis provides an opportunity to maximize free cooling hours throughout the year. There might be some otherwise ignored and discrete sources of particle origin like settled dust in the HVAC ducts and ionic residues in the evaporative cooling media pads which might reach the IT equipment along with the airflow. For HVAC ducts, it is concluded that the particle deposition increases with increasing velocity for coarse particles [165]. This deposition reduces with increasing velocity for fine and submicron particles. This deposition mainly occurs due to the gravitational setting for heavy particles and turbulence effects in the subviscous laminar layer for submicron particles. Boundary layer separation at bends and corners causing flow circulation is also an important parameter in particle deposition in ducts and around bluff bodies.

It can be observed from the reviewed literature that there are still a lot of potential research opportunities that can lead to a more reliable computing environment inside the data centers that implement airside economization. These areas include utilizing and improving particle and gas-phase filtration systems and revising the existing cleanliness standards as per current and ever-increasing computing and reliability needs. Monitoring measures like gas analyzers can aid in predicting the chemical gaseous composition present in the surrounding environment. Greater emphasis should be laid upon field test results for multiple data center sites especially I polluted geographies and regions with high sea-salt content. In doing so, a good estimate of failure x-factors can be obtained which can depict an upper limit of operating conditions for the datacom equipment. It is also highly imperative to classify the data centers using corrosion classification silver or copper coupons with ISA severity level G2 or G3. Another measure that can be taken at the manufacturer's end is utilizing field data related to the reliability and performance of the components rather than that in a laboratory simulated environment.

Funding Data

- NSF IUCRC (Award No. IIP-1738811; Funder ID: 10.13039/100000001).

Nomenclature

ACU = air conditioning unit
Ag = silver
ANSI = American Nation Standards Institute
ASE = airside economization
ASHRAE = American Society of Heating, Refrigerating and Air-conditioning Engineers
ASTM = American Society for Testing and Material
Au = gold
CAC = cold aisle containment
CFD = computational fluid dynamics
CRAC = computer room air conditioning
CRH = critical relative humidity
Cu = copper
DRH = déliquescent relative humidity
ECM = electrochemical migration
EDS = Electronic Industries Association
EIA = gold on electrodeless nickel
ENIG = environmental scanning electron microscope
EPMA = electron probe microanalysis
E-SEM = environmental scanning electron microscope
FoS = flowers of sulfur
HDD = hard disk drive
I/DEC = indirect/direct evaporative cooling
IEC = International Electrotechnical Commission
ImAg = immersion silver
ImSn = immersion tin
iNEMI = International Electronics Manufacturers Initiative
ISA = International Standards Association
ITE = information technology equipment
mA = milli-ampere
MEMS = microelectronics and microsystems
MERV = maximum efficiency rating value
MFG = mixed flowing gas
MMT = measurement and management technologies
mV = milli-volt
Ni = nickel
OSP = organic surface preservative
Pb = lead
PCB = printed circuit board
Pd = palladium
PDU = power distribution unit
Ppb = parts per billion

ppm = parts per million
RANS = Reynolds-averaged Navier–Stokes
RH = relative humidity
RoHS = restriction of hazardous substance
RPM = revolutions per minute
SIR = surface insulation resistance
Sn = tin
TEM = transmission electron microscopy
UPS = universal power supply
XRPD = X-ray powder diffraction

References

[1] Buyya, R., Vecchiola, C., and Selvi, S. T., 2013, "Mastering Cloud Computing: Foundations and Applications Programming," Morgan Kaufmann, Burlington, MA.

[2] Buyya, R., Beloglazov, A., and Abawajy, J., 2010, "Energy-Efficient Management of Data Center Resources for Cloud Computing: A Vision, Architectural Elements, and Open Challenges," Proceedings of the International Conference on Parallel and Distributed Processing Techniques and Applications (PDPTA 2010), Las Vegas, NV, July 12–15.

[3] Krug, L., Shackleton, M., and Saffre, F., 2014, "Understanding the Environmental Costs of Fixed Line Networking," Proceedings of the Fifth International Conference on Future Energy Systems, Cambridge, UK, June 11–13, pp. 87–95 .

[4] Shehabi, A., Smith, S. J., Sartor, D. A., Brown, R. E., Herrlin, M., Koomey, J. G., Masanet, E. R., Horner, N., Azevedo, I. L., and Lintner, W., 2016, "United States Data Center Energy Usage Report," Lawrence Berkeley National Laboratory, Berkeley, CA, Report No. LBNL-1005775.

[5] Koomey, J., 2011, "Growth in Data Center Electricity Use 2005 to 2010," A Report by Analytical Press, Completed at the Request of The New York Times, Analytics Press, El Dorado Hills, CA, p. 161.

[6] Rong, H., Zhang, H., Xiao, S., Li, C., and Hu, C., 2016, "Optimizing Energy Consumption for Data Centers," Renewable Sustain. Energy Rev., **58**, pp. 674–691.

[7] Zhou, R., Wang, Z., Bash, C. E., and McReynolds, A., 2011, "Modeling and Control for Cooling Management of Data Centers With Hot Aisle Containment," ASME Paper No. IMECE2011-62506.

[8] ASHRAE, 2015, "Thermal Guidelines for Data Processing Environments," ASHRAE Datacom Series, 4th ed., ASHRAE Inc, Atlanta, GA.

[9] Patterson, M. K., Atwood, D., and Miner, J. G., 2009, "Evaluation of Air-Side Economizer Use in a Compute-Intensive Data Center," ASME Paper No. InterPACK2009-89358.

[10] Lee, K. P., and Chen, H. L., 2013, "Analysis of Energy Saving Potential of Air-Side Free Cooling for Data Centers in Worldwide Climate Zones," Energy Build., **64**, pp. 103–112.

[11] ASHRAE ANSI/ASHRAE/IES Standard 90.1, 2019, "Energy Standard for Buildings Except for Low-Rise Residential Buildings," ASHRAE, Atlanta, GA.

[12] OUC, 2019, "Economizers,"OUC, accessed Dec. 20, 2019, https://ouc.bizenergyadvisor.com/article/economizers

[13] Intel Information Technology, 2008, "Reducing Data Center Cost With an Air Economizer," IT@Intel Brief; Computer Manufacturing; Energy Efficiency, accessed June 7, 2021, https://www.intel.com/content/dam/doc/technology-brief/data-center-efficiency-xeon-reducing-data-center-cost-with-air-economizer-brief.pdf

[14] ISA, 1985, "Environmental Conditions for Process Measurement and Control Systems: Airborne Contaminants," ISA-The Instrumentation Systems, and Automation Society, Research Triangle Park, NC, Standard No. ISA-71.04-1985.

[15] Cole, M., Hedlund, L., Hutt, G., Kiraly, T., Klein, L., Nickel, S., Singh, P., and Tofil, T., 2010, "Harsh Environment Impact on Resistor Reliability," SMTAI Conference Proceedings, Orlando, FL, Oct. 24–28, pp. 1–9.

[16] Official Journal of the European Union, 2003, "Directive 2002/95/EC of the European Parliament and of the Council of 27 January 2003 on the Restriction of the Use of Certain Hazardous Substances in Electrical and Electronic Equipment," Official Journal of the European Union, Luxembourg, pp. L37/19–23.

[17] Fu, H., Chen, C., Singh, P., Zhang, J., Kurella, A., Chen, X., Jiang, X., Burlingame, J., and Lee, S., 2012, "Investigation of Factors That Influence Creep Corrosion on Printed Circuit Boards," SMTA Pan Pacific Microelectronics Symposium, Kauai, HI, Feb. 14–16, pp. 14–16.

[18] Fu, H., Chen, C., Singh, P., Zhang, J., Kurella, A., Chen, X., Jiang, X., Burlingame, J., and Lee, S., 2012, "Investigation of Factors That Influence Creep Corrosion on Printed Circuit Boards-Part 2," Proceedings of SMTA International, Olando, FL, Oct. 14–18, pp. 292–299.

[19] Ready, W. J., Turbini, L. J., Nickel, R., and Fischer, J., 1999, "A Novel Test Circuit for Automatically Detecting Electrochemical Migration and Conductive Anodic Filament Formation," J. Elect. Mater., **28**(11), pp. 1158–1163.

[20] Ailor, W., Dean, S., and Haynie, F., 1974, "Corrosion in Natural Environments," Presented at the Seventy-Sixth Annual Meeting American Society For Testing and Materials, ASTM Special Technical Publication 558, Philadelphia, PA, June 24–29, pp. 7–21.

[21] Rice, D. W., Peterson, P., Rigby, E. B., Phipps, P. B. P., Cappell, R. J., and Tremoureux, R., 1981, "Atmospheric Corrosion of Copper and Silver," J. Electrochem. Soc., **128**(2), pp. 275–284.

[22] W. H. Abbott, 1989, "The Corrosion of Copper and Porous Gold in Flowing Mixed Gas Environments," Proceedings of the Thirty Fifth Meeting of the IEEE Holm Conference on Electrical Contacts, Chicago, IL, Sept. 18–20, pp. 141–146.

[23] Leygraf, C., Wallinder, I. O., Tidblad, J., and Graedel, T., 2016, "*Atmospheric Corrosion*," John Wiley & Sons, New York.

[24] ASHRAE, T.C. 9.9, 2013, "Particulate and Gaseous Contamination in Datacom Environments" ASHRAE, Atlanta, GA.

[25] Muller, C., 2014, "Reliability Concerns for Data Center ITE: Contamination Issues, Standards Actions, and Case Studies," IPC APEX Conference & Exhibition, Las Vegas, NV, Mar. 23–27.

[26] Shah, J. M., 2016, "Reliability Challenges in Airside Economization and Oil Immersion Cooling," M.S. dissertation, The University of Texas at Arlington, Arlington, TX.

[27] Singh, P., Ruch, P., Saliba, S., and Muller, C., 2015, "Characterization, Prevention and Removal of Particulate Matter on Printed Circuit Boards," IPC APEX, San Diego, CA.

[28] Geng, H., and Han, T., 2014, "Particulate and Gaseous Contamination in Data Centers," Data Center Handbook, H. Geng, ed., John Wiley & Sons, New York, pp. 307–312.

[29] Purafil, 2020, "Causes of Corrosion and Corrosion Monitoring," Purafil, Doraville, GA, accessed Jan. 19, 2020, https://www.purafil.com/causes-corrosion-corrosion-monitoring/

[30] Zhang, J., Zhang, R., Schmidt, R., Gilbert, J., and Guo, B., 2019, "Impact of Gaseous Contamination and High Humidity on the Reliable Operation of Information Technology Equipment in Data Centers (1755-TRP)," ASHRAE, Atlanta, GA, Report No. D-RP-1755.

[31] Buchard, V., Da Silva, A. M., Colarco, P., Krotkov, N., Dickerson, R. R., Stehr, J. W., Mount, G., Spinei, E., Arkinson, H. L., and He, H., 2014, "Evaluation of GEOS-5 Sulfur Dioxide Simulations During the Frostburg, MD 2010 Field Campaign," Atmos. Chem. Phys., **14**(4), pp. 1929–1941.

[32] Song, B., Azarisn, M. H., and Pecht, M. G., 2013, "Effect of Temperature and Relative Humidity on the Impedance Degradation of Dust-Contaminated Electronics," J. Electrochem. Soc., **160** (3), pp. C97–C105.

[33] Seinfeld, J. H., and Pandis, S. N., 2016, "Atmospheric Chemistry and Physics: From Air Pollution to Climate Change," John Wiley & Sons, New York.

[34] Zhao, P. S., Fan Dong, Di He, X. J. Zhao, W. Z. Zhang, Q. Yao, and H. Y. Liu., 2013, "Characteristics of Concentrations and Chemical Compositions for PM 2.5 in the Region of Beijing, Tianjin, and Hebei, China," Atmos. Chem. Phys., **13**, pp. 4631–4644.

[35] U. S. Environmental Protection Agency, 2014, "Air Trends 1995 Summary – Nitrogen Dioxide (NO_2)," U. S. Environmental Protection Agency, Researech Park Triangle, NC, accessed Jan. 30, 2020, http://www.epa.gov/airtrends/aqtrnd95/no2.html

[36] Anand, R., 2018, "Development and Validation of the Deliquescent Relative Humidity Test Method for the Accumulated Particulate Matter Found in a Data Center Utilizing an Airside Economizer," M.S. dissertation, The University of Texas at Arlington, Arlington, TX.

[37] Thirunavakkarasu, G., 2018, "Air Flow Pattern and Path Flow Simulation of Airborne Particulate Contaminants in a Cold-Aisle Containment High-Density Data Center Utilizing Airside Economization," M.S. dissertation, The University of Texas at Arlington, Arlington, TX.

[38] Saini, S., 2018, "Airflow Path and Flow Pattern Analysis of Sub-Micron Particulate Contaminants in a Data Center with Hot Aisle Containment System Utilizing Direct Air Cooling," M.S. dissertation, The University of Texas at Arlington, Arlington, TX.

[39] Comizzoli, R. B., Frankenthal, R. P., Lobnig, R. E., and Peins, G., 1993, "Corrosion of Electronic Materials and Devices by Submicron Atmospheric Particles," Electrochem. Soc., Interface, **2**(3), pp. 26–33.

[40] The United States Environmental Protection Agency, 2004, "The Particle Pollution Report-Current Understanding of Air Quality and Emissions through 2003," The United States Environmental Protection Agency, Research Park Triangle, NC, Report No. EPA 454-R-04-002, pp. 1–12.

[41] Shah, J. M., Awe, O., Agarwal, P., Akhigbe, I., Agonafer, D., Singh, P., Kannan, N., and Kaler, M., 2017, "Qualitative Study of Cumulative Corrosion Damage of IT Equipment in a Data Center Utilizing Air-Side Economizer," ASME Paper No. IMECE2016-66199.

[42] IPC Handbook, 1990, "Surface Insulation Resistance Handbook," IPC Handbook, Northbrook, IL, Report No. IPC-9201.

[43] Zhan, S., Azarian, M. H., and Pecht, M. G., 2006, "Surface Insulation Resistance of Conformally Coated Printed Circuit Boards Processed with No-Clean Flux," IEEE Trans. Elect. Packag. Manufact., **29**(3), pp. 217–223.

[44] Zhong, X., Chen, L., Medgyes, B., Zhang, Z., Gao, S., and Jakab, L., 2017, "Electrochemical Migration of Sn and Sn Solder Alloys: A Review," RSC Adv., **7**(45), pp. 28186–28206.

[45] Yang, S., and Christou, A., 2007, "Failure Model for Silver Electrochemical Migration," IEEE Trans. Dev. Mater. Reliab., **7**(1), pp. 188–196.

[46] Zhou, Y., Yang, P., Yuan, C., and Huo, Y., 2013, "Electrochemical Migration Failure of the Copper Trace on Printed Circuit Board Driven by Immersion Silver Finish," Chem. Eng. Trans., **33**, pp. 559–564.

[47] Coleman, M. V., and Winster, A. E., 1981, "Silver Migration in Thick Film Conductors and Chip Attachment Resins," Microelectron. J., **12**(4), pp. 23–29.

[48] Yang, S., Wu, J., and Christou, A., 2006, "Initial Stage of Silver Electrochemical Migration Degradation," Microelectron. Reliab., **46**(9–11), pp. 1915–1921.

[49] Li, Y., and Wong, C. P., 2006, "Monolayer Protection for Electrochemical Migration Control in Silver Nanocomposite," Appl. Phys. Lett., **89**(11), p. 112.

[50] Yoo, Y. R., Nam, H. S., Jung, J. Y., Lee, S. B., Park, Y. B., Joo, Y. C., and Kim, Y. S., 2007, "Effects of Ag and Cu Additions on the Electrochemical Migration Susceptibility of Pb-Free Solders in Na2SO4 Solution," Corr. Sci. Technol., **6**(2), pp. 50–55.
[51] Minzari, D., Jellesen, M. S., Møller, P., and Ambat, R., 2011, "On the Electrochemical Migration Mechanism of Tin in Electronics," Corros. Sci., **53**(10), pp. 3366–3379.
[52] Minzari, D., Grumsen, F. B., Jellesen, M. S., Møller, P., and Ambat, R., 2011, "Electrochemical Migration of Tin in Electronics and Microstructure of the Dendrites," Corros. Sci., **53**(5), pp. 1659–1669.
[53] Ambat, R., Jellesen, M. S., Minzari, D., Rathinavelu, U., Johnsen, M. A., Westermann, P., and Møller, P., 2009, "Solder Flux Residues and Electrochemical Migration Failures of Electronic Devices," Proceedings of the EUROCORR, Nice, France, Sept. 6–10, Paper No. 8141.
[54] Minzari, D., Jellesen, M. S., Moller, P., Wahlberg, P., and Ambat, R., 2009, "Electrochemical Migration on Electronic Chip Resistors in Chloride Environments," IEEE Trans. Dev. Mater. Reliab., **9**(3), pp. 392–402.
[55] Verdingovas, V., Jellesen, M. S., and Ambat, R., 2013, "Influence of Sodium Chloride and Weak Organic Acids (Flux Residues) on Electrochemical Migration of Tin on Surface Mount Chip Components," Corros. Eng., Sci. Technol., **48**(6), pp. 426–435.
[56] Zhan, S., Azarian, M. H., and Pecht, M., 2008, "Reliability of Printed Circuit Boards Processed Using No-Clean Flux Technology in Temperature–Humidity–Bias Conditions," IEEE Trans. Dev. Mater. Reliab., **8**(2), pp. 426–434.
[57] Natsui, M., Asakawa, H., Tanaka, T., Ohki, Y., Maeno, T., and Okamoto, K., 2011, "Generation Mechanism of Electrochemical Migration in Printed Wiring Board Insulation," IEEJ Trans. Elect. Electron. Eng., **6**(3), pp. 200–206.
[58] Komatsu, D., Takahashi, N., Furutani, T., Bhandari, R. K., Sato, K., Jinbo, N., and Kariya, T., 2011, "Mechanism Verification of Electrochemical Migration of Fine Cu Wiring," Jpn. J. Appl. Phys., **50**(5S1), p. 05EA10.
[59] Kim, J. H., and Park, S. D., 2013, "Acceleration of Applied Voltage on Metallic Ion Migration of Wires in NTC Thermistor Temperature Sensors," Eng. Fail. Anal., **28**, pp. 252–263.
[60] He, X., Azarian, M. H., and Pecht, M. G., 2014, "Analysis of the Kinetics of Electrochemical Migration on Printed Circuit Boards Using Nernst-Planck Transport Equation," Electrochim. Acta, **142**, pp. 1–10.
[61] Medgyes, B., Illés, B., and Harsányi, G., 2012, "Electrochemical Migration Behaviour of Cu, Sn, Ag and Sn63/Pb37," J. Mater. Sci.: Mater. Electron., **23**, pp. 551–556.
[62] Huang, H. L., Pan, Z. Q., Guo, X. P., and Qiu, Y. B., 2014, "Effects of Direct Current Electric Field on Corrosion Behaviour Of Copper, Cl− Ion Migration Behaviour and Dendrites Growth Under Thin Electrolyte Layer," Trans. Nonferrous Metals Soc. China, **24**(1), pp. 285–291.
[63] Harsanyi, G., 1995, "Electrochemical Processes Resulting in Migrated Short Failures in Microcircuits," IEEE Trans. Compon. Packag. Manufact. Technol. Part A, **18**(3), pp. 602–610.
[64] Sbar, N., 1976, "Bias-Humidity Performance of Encapsulated and Unencapsulated Ti-Pd-Au Thin-Film Conductors in an Environment Contaminated With Cl_2," IEEE Trans. Parts, Hybrids, Packag., **12**(3), pp. 176–181.
[65] Brambilla, E., Brambilla, P., Canali, C., Fantini, F., and Vanzi, M., 1983, "Anodic Gold Corrosion in Plastic Encapsulated Devices," Microelectron. Reliab., **23**(3), pp. 577–585.
[66] D. W. Rice, R. J. Cappell, P. B. P. Phipps and P. Peterson, 1982, "Indoor Atmospheric Corrosion of Copper, Nickel, Cobalt, and Iron, in Atmospheric Corrosion," W. H. Ailor, ed., Wiley, New York.
[67] Hillman, C., Arnold, J., Binfield, S., and Seppi, J., 2007, "Silver and Sulfur: Case Studies, Physics and Possible Solutions," Proceedings of SMTA International, Orlando, FL, Oct. 7–11, pp. 620–632.
[68] Kohman, G. T., Hermance, H. W., and Downes, G. H., 1955, "Silver Migration in Electrical Insulation," Bell Syst. Tech. J., **34**(6), pp. 1115–1147.
[69] Steppan, J. J., Roth, J. A., Hall, L. C., Jeannotte, D. A., and Carbone, S. P., 1987, "A review of Corrosion Failure Mechanisms During Accelerated Tests: Electrolytic Metal Migration," J. Electrochem. Soc., **134**(1), pp. 175–190.
[70] Lin, J. C., and Chuang, J. Y., 1997, "Resistance to Silver Electrolytic Migration for Thick-Film Conductors Prepared from Mixed and Alloyed Powders of Ag-15Pd and Ag-30Pd," J. Electrochem. Soc., **144**(5), p. 1652.
[71] Naguib, H., and MacLaurin, B., 1979, "Silver Migration and the Reliability of Pd/Ag conductors in Thick-Film Dielectric Crossover Structures," IEEE Trans. Compon. Hybrids, Manuf. Technol., **2**(2), pp. 196–207.
[72] Sease, C., Selwyn, L. S., Zubiate, S., Bowers, D. F., and Atkins, D. R., 1997, "Problems with Coated Silver: Whisker Formation and Possible Filiform Corrosion," Stud. Conserv., **42**(1), pp. 1–10.
[73] Daniels, V., and Ward, S., 1982, "A Rapid Test for the Detection of Substances Which Will Tarnish Silver," Stud. Conserv., **27**(2), pp. 58–60.
[74] McNeilL, M. B., and Little, B. J., 1992, "Corrosion Mechanisms for Copper and Silver Objects in Near-Surface Environments," J. Am. Inst. Conserv., **31**(3), pp. 355–366.
[75] S. C. Axtell, 2002, "Failure of Thick Chip Resistor in Sulphur Containing Environments," Microelectronic Failure Analysis: Desk Reference 2002 Supplement (ASM International), pp. 161–173.
[76] ASHRAE, 2013, "Particulate and Gaseous Contamination Guidelines for Data Centers," 2nd ed., ASHRAE Datacom Series, ASHRAE, Atlanta, GA.
[77] Singh, P., Zhang, Z. Q., Kuo, G. U., and Luo, G., 2009, IBM Corporation, Private Communication.
[78] ANSI/ISA, 2013, "Environmental Conditions for Process Measurement and Control Systems: Airborne Contaminants," The Instrumentation, Systems, and Automation Society, Report No. ANSI/ISA-71.04-2013.
[79] Reid, M., Punch, J., Ryan, C., Franey, J., Derkits, G. E., Reents, W. D., and Garfias, L. F., 2007, "The Corrosion of Electronic Resistors," IEEE Trans. Compon. Packag. Technol., **30**(4), pp. 666–672.
[80] Shah, J. M., 2018, "Characterizing Contamination to Expand ASHRAE Envelope in Airside Economization and Thermal and Reliability in Immersion Cooling of Data Centers," Ph.D. dissertation, The University of Texas at Arlington, Arlington, TX.
[81] Huang, H., Dong, Z., Chen, Z., and Guo, X., 2011, "The Effects of Cl− Ion Concentration and Relative Humidity on Atmospheric Corrosion Behaviour of PCB-Cu Under Adsorbed Thin Electrolyte Layer," Corros. Sci., **53**(4), pp. 1230–1236.
[82] Zhang, S. N., Osterman, M., Shrivastava, A., Kang, R., Pecht, M. G., 2010, "The Influence of H2S Exposure on Immersion-Silver-Finished PCBs Undermixed-Flow Gas Testing," IEEE Trans. Dev. Mater. Reliab., **10**(1), pp. 71–81.
[83] Gen, W., Chen, X., Hu, A., and Li, M., 2011, "Effect of Ag on Oxidation of Cu-Base Leadframe," Microelectron. Reliab., **51**(4), pp. 866–870.
[84] Zhao, P., and Pecht, M., 2003, "Field Failure Due to Creep Corrosion on Components with Palladium Pre-Plated Leadframes," Microelectron. Reliab., **43**(5), pp. 775–783.
[85] Huang, H., Guo, X., Zhang, G., and Dong, Z., 2011, "The Effects of Temperature and Electric Field on Atmospheric Corrosion Behaviour of PCB-Cu Under Absorbed Thin Electrolyte Layer," Corros. Sci., **53**(5), pp. 1700–1707.
[86] Verdingovas, V., Jellesen, M. S., and Ambat, R., 2013, "Influence of Sodium Chloride and Weak Organic Acids (Flux Residues) on Electrochemical Migration of Tin on Surface Mount Chip Components," Corros. Eng., Sci. Technol., **48**(6), pp. 426–435.
[87] Zou, S., Li, X., Dong, C., Ding, K., & Xiao, K., 2013, "Electrochemical Migration, Whisker Formation, and Corrosion Behavior of Printed Circuit Board Under Wet H2S Environment," Electrochim. Acta, **114**, pp. 363–371.
[88] Kleber, C., Wiesinger, R., Schnöller, J., Hilfrich, U., Hutter, H., and Schreiner, M., 2008, "Initial Oxidation of Silver Surfaces by S2− and S4+ Species," Corros. Sci., **50**(4), pp. 1112–1121.
[89] Tran, T. T. M., Fiaud, C., and Sutter, E. M. M., 2005, "Oxide and Sulphide Layers on Copper Exposed to H2S Containing Moist Air," Corros. Sci., **47**(7), pp. 1724–1737.
[90] Krumbein, S., 1969, "Corrosion Through Porous Gold Plate," IEEE Trans. Parts, Mater. Packag., **5**(2), pp. 89–98.
[91] Russo, S. G., Henderson, M. J., and Hinton, B. R. W., 2002, "Corrosion of An Aircraft Radar Antenna Waveguide," Eng. Fail. Anal., **9**(4), pp. 423–434.
[92] Huang, H., Guo, X., Zhang, G., and Dong, Z., 2011, "Effect of Direct Current Electric Field on Atmospheric Corrosion Behavior of Copper Under Thin Electrolyte Layer," Corros. Sci., **53**(10), pp. 3446–3449.
[93] Gil, H., Calderón, J. A., Buitrago, C. P., Echavarría, A., and Echeverría, F., 2010, "Indoor Atmospheric Corrosion of Electronic Materials in Tropical-Mountain Environments," Corros. Sci., **52**(2), pp. 327–337.
[94] Desmarest, S. G., 2012, "Reliability of Pb-Free Solders for Harsh Environment Electronic Assemblies," Mater. Sci. Technol., **28**(3), pp. 257–273.
[95] Chen, C., Lee, J. C., Chang, G., Lin, J., Hsieh, C., Liao, J., and Huang, J., 2012, "The Surface Finish Effect on the Creep Corrosion in PCB," IPC APEX EXPO Technical Conference Proceedings, San Diego, CA, Feb. 28.
[96] Singh, P., Palmer, L., Fu, H., Lee, D., and Lee, J., 2017, "Round Robin Testing of Creep Corrosion Dependence on Relative Humidity," SMTA International, Rosemont, IL.
[97] Graedel, T. E., Nassau, K., and Franey, J. P., 1987, "Copper Patinas Formed in the Atmosphere—I. Introduction," Corros. Sci., **27**(7), pp. 639–657.
[98] Graedel, T. E., 1987, "Copper Patinas Formed in the Atmosphere—III. A Semi-Quantitative Assessment of Rates and Constraints in the Greater New York Metropolitan Area," Corros. Sci., **27**(7), pp. 741–769.
[99] Muller, A. J., and McCrory-Joy, C., 1987, "Chromatographic Analysis of Copper Patinas Formed in the Atmosphere," Corros. Sci., **27**(7), pp. 695–701.
[100] Nassau, K., Gallagher, P. K., Miller, A. E., and Graedel, T. E., 1987, "The Characterization of Patina Components by X-Ray Diffraction and Evolved Gas Analysis," Corros. Sci., **27**(7), pp. 669–684.
[101] Vernon, W. H. J., 1935, "A Laboratory Study of the Atmospheric Corrosion of Metals. Part II—Iron: The Primary Oxide Film. Part III—The Secondary Product or Rust (Influence of Sulphur Dioxide, Carbon Dioxide, and Suspended Particles on the Rusting of Iron)," Trans. Faraday Soc., **31**, pp. 1668–1700.
[102] Abbott, W., 1974, "Effects of Industrial Air Pollutants on Electrical Contact Materials," IEEE Trans. Parts, Hybrids, Packag., **10**(1), pp. 24–27.
[103] Sharma, S. P., 1978, "Atmospheric Corrosion of Silver, Copper, and Nickel—Environmental Test," J. Electrochem. Soc., **125**(12), pp. 2005–2011.
[104] Valdez Salas, B., Schorr Wiener, M., Zlatev Koytchev, R., López Badilla, G., Ramos Irigoyen, R., Carrillo Beltrán, M., Radnev Nedev, N., Curiel Alvarez, M., Rosas Gonzalez, N., and Bastidas Rull, J. M., 2013, "Copper Corrosion by Atmospheric Pollutants in the Electronics Industry," Int. Schol. Res. Not., p. 7.
[105] Veleva, L., Valdez, B., Lopez, G., Vargas, L., and Flores, J., 2008, "Atmospheric Corrosion of Electro-Electronics Metals in Urban Desert Simulated Indoor Environment," Corros. Eng., Sci. Technol., **43**(2), pp. 149–155.

[106] Pujara, K., 2015, "The Effect of Temperature and Relative Humidity on the Corrosion Rates of Copper and Silver in Electronic Equipment in the Presence of Sulfur Environment," M.S. dissertation, The University of Texas at Arlington, Arlington, TX.
[107] Abbott, W. H., 1985, "Field Vs Laboratory Experience in the Evaluation of Electronic Components and Materials," Mater. Perform., **24**(8), pp. 46–50.
[108] Abbott, W. H., 1987, "Corrosion of Porous Gold Plating in Field and Laboratory Environments," Plat. Surf. Finish., **74**(11), pp. 72–75.
[109] Abbott, W. H., 1988, "The Development and Performance Characteristics of Mixed Flowing Gas Test Environment," IEEE Trans. Compon. Hybrids, Manuf. Technol., **11**(1), pp. 22–35.
[110] Abbott, W. H., 1965, "The Measurement of Equipment Operating Environments to Evaluate Corrosion Related Failure Mechanisms," IEC Document 65, Montreal, PQ, Canada.
[111] Abbott, W., 1986, "The Corrosion of Porous Gold Plating," Proceedings of 13th ICEC, Lausanne, Switzerland.
[112] Rice, D. W., 1985, "Corrosion in The Electronics Industry," Corrosion/85, March 1985, Boston, MA, Paper No. 323.
[113] Zhang, S., Shrivastava, A., Osterman, M., Pecht, M., and Kang, R., 2009, "The Influence of SO_2 Environments on Immersion Silver Finished PCBs by Mixed Flow Gas Testing," International Conference on Electronic Packaging Technology & High Density Packaging, Beijing, China, Aug. 10–13, pp. 116–122.
[114] Cullen D., 2005, "Surface Tarnish and Creeping Corrosion on Pb-free Circuit Board Surface Finishes," IPC Works, Las Vegas, NV, Oct. 20–22.
[115] Veale, R., 2005, "Reliability of PCB Alternate Surface Finishes in a Harsh Industrial Environment," Proceedings of SMTA International, Rosemont, IL, Sept. 25–29, pp. 494–499.
[116] Mazurkiewicz, P., 2006, "Accelerated Corrosion of Printed Circuit Boards Due To High Levels of Reduced Sulfur Gasses in Industrial Environments," Proceedings of 32nd International Symposium for Testing and Failure Analysis, Austin, TX, Nov. 12–16, pp. 469–477.
[117] Xu, C., Flemming, D., Demerkin, K., 2007, "Corrosion Resistance of PCB Surface Finishes," Alcatel-Lucent, Apex, Los Angeles, CA, pp. 20–22.
[118] Zhao, P., Pecht, M. G., Kang, S., and Park, S., 2006, "Assessment of Ni/Pd/Au–Pd and Ni/Pd/Au–Ag Preplated Leadframe Packages Subject to Electrochemical Migration and Mixed Flowing Gas Tests," IEEE Trans. Compon. Packag. Technol., **29**(4), pp. 818–826.
[119] Williams, D. W., 1988, "The Effect of Test Environment on the Creep of Base Metal Surface Films Over Precious Metal Inlays," IEEE Trans. Compon. Hybrids Manuf. Technol., **11**(1), pp. 36–42.
[120] Li, J., Broas, M., Raami, J., Mattila, T. T., and Paulasto-Kröckel, M., 2014, "Reliability Assessment of a MEMS Microphone Under Mixed Flowing Gas Environment and Shock Impact Loading," Microelectron. Reliab., **54**(6–7), pp. 1228–1234.
[121] Hannigan, K., Reid, M., Collins, M. N., Dalton, E., Xu, C., Wright, B., Demirkan, K., Opila, R. L., Reents, W. D., Franey, J. P., and Fleming, D. A., 2012, "Corrosion of RoHS-Compliant Surface Finishes in Corrosive Mixed Flowing Gas Environments," J. Electron. Mater., **41**(3), pp. 611–623.
[122] Reid, M., Punch, J., Grace, G., Garfias, L. F., and Belochapkine, S., 2006, "Corrosion Resistance of Copper-Coated Contacts," J. Electrochem. Soc., **153**(12), p. B513.
[123] Martens, R., and Pecht, M. G., 2000, "An Investigation of the Electrical Contact Resistance of Corroded Pore Sites on Gold Plated Surfaces," IEEE Trans. Adv. Packag., **23**(3), pp. 561–567.
[124] Maul, C., McBride, J. W., and Swingler, J., 2001, "Intermittency Phenomena in Electrical Connectors," IEEE Trans. Compon. Packag. Technol., **24**(3), pp. 370–377.
[125] ASTM, 2013, "Standard Test Method for Porosity in Metallic Coatings by Humid Sulfur Vapor ("Flowers-of-Sulfur")," ASTM International, West Conshohocken, PA, Standard No. B809-95.
[126] Mahadeo, D. M., 2015, "Copper Corrosion in the Flowers of Sulfur Test Environment," Ph.D. dissertation, University of Maryland, College Park, MD.
[127] Hindin, B., Fernandez, J., and Magnetics, P., 2003, "Testing of Conformal Coatings Using the Flowers-of-Sulfur Test," Tri-Service Corrosion Conference, pp. 17–21.
[128] Hindin, B. S., Kremser, D., and Pledger, M., 2015, "Silver Sulfidation Kinetics in Sulfur-Bearing Environments," Paper presented at the CORROSION 2015, Dallas, TX, Paper No. NACE-2015-5791.
[129] Reid, M., Collins, M. N., Dalton, E., Punch, J., and Tanner, D. A., 2012, "Testing Method for Measuring Corrosion Resistance of Surface Mount Chip Resistors," Microelectron. Reliab., **52**(7), pp. 1420–1427.
[130] Singh, Fabry, P., M., Green, W. B., 2017, "Flowers of Sulfur Creep Corrosion Testing of Populated Circuit Boards," Proceedings of IPC APEX EXPO, San Diego, CA, Feb. 11–16, pp. 1–6.
[131] Fu, H., Singh, P., Campbell, L., Zhang, J., Ables, W., Lee, D., Lee, J., Li, J., Zhang, S., and Lee, S., 2014, "Testing Printed Circuit Boards for Creep Corrosion in Flowers of Sulfur Chamber," Proceedings of IPC APEX Expo, Las Vegas, NV, Mar. 25–27, pp. 25–27.
[132] Fu, H., S., Singh, C. P., Guo, K., Li, J., Lee, S., and Tong, G., 2015, "Testing Printed Circuit Boards for Creep Corrosion in Flowers of Sulfur Chamber: Phase 2A," Proceedings of IPC APEX Expo, San Diego, CA, Feb. 24–26.
[133] Fu, H., Singh, P., Kazi, A., Ables, W., Lee, D., Lee, J., Guo, K., Li, J., Lee, S., Tong, G., 2015, "Testing Printed Circuit Boards for Creep Corrosion in Flowers of Sulfur Chamber: Phase 2," SMTA Int'l, Rosemont, IL, Sept. 27–Oct. 1.
[134] Singh, P., Palmer, L., Lee, D., Lee, J., Guo, K., Liu, J., Lee, S., Tong, G., Xu, C., Fleming, D., and Fu, H., 2017, "Relative Humidity Dependence of Creep Corrosion on Printed Circuit Boards," International Conference on Electronics Packaging (ICEP), Yamagata, Japan, Apr. 19–22, pp. 41–46.
[135] Singh, P., Cole, M., Kiraly, T., Tan, J., Rangaraj, R., Wood, G., and Chang, T., 2016, "Comparing Flowers of Sulfur and Mixed Flowing Gas Creep Corrosion Testing of Printed Circuit Boards," SMTA International, Rosemont, IL, Sept. 25–29, pp. 25–29.
[136] Singh, P., Fabry, M., and Green, W. B., 2017, "Flowers of Sulfur Creep Corrosion Testing of Populated Circuit Boards," Proceedings of IPC APEX Expo, San Diego, CA, Feb. 12–16, pp. 13–16.
[137] Muller, C., 2010, "What's Creeping Around in Your Data Center?," ASHRAE 2010 Winter Conference (OR-10-023), Orlando, FL, Jan. 23–27, pp. 207–222.
[138] Muller, C. O., 1991, "Multiple Contaminant Gas Effects on Electronic Equipment Corrosion," Corrosion **47**(2), pp. 146–151.
[139] Hamann, H. F., van Kessel, T. G., Iyengar, M., Chung, J. Y., Hirt, W., Schappert, M. A., Claassen, A., Cook, J. M., Min, W., Amemiya, Y., and López, V., 2009, "Uncovering Energy-Efficiency Opportunities in Data Centers," IBM J. Res. Dev., **53**(3), pp. 1–12.
[140] Awe, O. M., "The Effects of Temperature and Relative Humidity on Exposure of Legacy and Future Technology Hardware, Under Real Data Center Conditions in an ANSI/ISA Classified G2 Environment," Ph.D. dissertation, The University of Texas at Arlington, Arlington, TX.
[141] IBM, 2020, "IBM Archives: IBM 350 Disk Storage Unit," IBM, Armonk, New York, Jan. 30, 2020, https://www.ibm.com/ibm/history/exhibits/storage/storage_350.html
[142] IBM, 1998, "OEM Hard Disk Drive Specifications for DDRS-39130/DDRS-34560 3.5-Inch Hard Disk Drive (9130/4560 MB) Revision (2.0)," IBM, Armonk, New York, accessed Jan. 30, 2020, http://ps-2.kev009.com/ohlandl/IBM_HD/ddrs_spw.pdf
[143] Khurshudov, A., and Waltman, R. J., 2001, "Tribology Challenges of Modern Magnetic Hard Disk Drives," Wear, **251**(1–12), pp. 1124–1132.
[144] Shah, H., 2013, "Gaseous Corrosion In Hard Disk Drive: A Computational Study," Master's thesis, The University of Texas at Arlington, Arlington, TX.
[145] Bagul, T., Pujara, K., Shah, J., Awe, O., & Agonafer, D., 2015, "Computational Study of Behavior of Gas Absorption in Data Center Equipment and its Effects on the Rate of Corrosion/Contamination," ASME Paper No. IPACK2015-48049.
[146] Dai, J., Das, D., and Pecht, M., 2012, "Prognostics-Based Risk Mitigation for Telecom Equipment Under Free Air Cooling Conditions," Appl. Energy, **99**, pp. 423–429.
[147] Atwood, D., and Miner, J. G., 2008, "Reducing Data Center Cost with an Air Economizer," White Paper: Intel Corporation, Santa Clara, CA, accessed Jan. 20, 2020, https://www.intel.com/content/dam/doc/technology-brief/data-center-efficiency-xeon-reducing-data-center-cost-with-air-economizer-brief. pdf
[148] Shah, J. M., Awe, O., Gebrehiwot, B., Agonafer, D., Singh, P., Kannan, N., and Kaler, M., 2017, "Qualitative Study of Cumulative Corrosion Damage of Information Technology Equipment in a Data Center Utilizing Air-Side Economizer Operating in Recommended and Expanded ASHRAE Envelope," ASME J. Electron. Packag., **139**(2), p. 020903.
[149] Shah, J. M., Misrak, A., Agonafer, D., and Kaler, M., 2019, "Identification and Characterization of Particulate Contaminants Found at a Data Center Using Airside Economization," ASME J. Electron. Packag., **141**(3), p. 031003.
[150] Awe, O., Shah, J. M., Agonafer, D., Singh, P., Kannan, N., and Kaler, M., 2020, "Experimental Description of Information Technology Equipment Reliability Exposed to a Data Center Using Airside Economizer Operating in Recommended and Allowable ASHRAE Envelopes in an ANSI/ISA Classified G2 Environment," ASME. J. Electron. Packag., **142**(2), p. 024501.
[151] Shah, J. M., Anand, R., Saini, S., Cyriac, R., Agonafer, D., Singh, P., and Kaler, M., 2019, "Development of a Technique to Measure Deliquescent Relative Humidity of Particulate Contaminants and Determination of the Operating Relative Humidity of a Data Center," ASME Paper No. IPACK2019-6601.
[152] Shah, J. M., Anand, R., Singh, P., Saini, S., Cyriac, R., Agonafer, D., and Kaler, M., 2020, "Development of a Precise and Cost-Effective Technique to Measure Deliquescent Relative Humidity of Particulate Contaminants and Determination of the Operating Relative Humidity of a Data Center Utilizing Airside Economization," ASME J. Electron. Packag., **142**(4), p. 041103.
[153] Adafruit, 2020, "Adafruit INA219 Current Sensor Breakout," Adafruit, New York, accessed Jan. 2020, https://learn.adafruit.com/adafruit-ina219-current-sensor-breakout
[154] Jones, P. J., and Whittle, G. E., 1992, "Computational Fluid Dynamics for Building Airflow Prediction—Current Status and Capabilities," Build. Environ., **27**(3), pp. 321–338.
[155] Chen, Q., and Zhang, Z., 2005, "Prediction of Particle Transport in Enclosed Environment," China Particuol., **3**(6), pp. 364–372.
[156] Seymour, M. J., Alani, A., Manning, A., and Jiang, J., 2000, "CFD Based Airflow Modelling to Investigate the Effectiveness of Control Methods Intended to Prevent the Transmission of Airborne Organisms," Proceedings of Roomvent 2000, Air Distribution in Rooms: Ventilation for Health and Sustainable Environment, Reading, UK, July 9–12, pp. 77–82.
[157] Thirunavakkarasu G., Satyam S., Shah, J. M., and Agonafer, D., 2018, "Air Flow Pattern and Path Flow Simulation of Airborne Particulate Contaminants in a High-Density Data Center Utilizing Airside Economization," ASME Paper No. IPACK2018-8436.
[158] Saini, S., Shahi, P., Bansode, P., Siddarth, A., Agonafer, D., 2020, "CFD Investigation of Dispersion of Airborne Particulate Contaminants in a Raised

Floor Data Center," 36th Semiconductor Thermal Measurement, Modeling & Management Symposium (SEMI-THERM), San Jose, CA, Mar. 16–20, pp. 39–47.
[159] QUARG, 1996, "Airborne Particulate Matter in the United Kingdom-Third QUARG Report," Urban Air Review Group, UK Air Information Resource, London, UK.
[160] Harrison, R., and Yin, J., 2004, "Characterisation of Particulate Matter in the United Kingdom," Report produced for Defra, the National Assembly for Wales, the Department of the Environment in Northern Ireland and the Scottish Executive, The University of Birmingham (REF. CPEA 6), Birmingham, UK.
[161] Čupr, P., Flegrová, Z., Franců, J., Landlová, L., and Klánová, J., 2013, "Mineralogical, Chemical and Toxicological Characterization of Urban Air Particles," Environ. Int., **54**, pp. 26–34.
[162] Frachtenberg, E., Lee, D., Magarelli, M., Mulay, V., and Park, J., 2012, "Thermal Design in the Open Compute Data Center," 13th InterSociety Conference on Thermal and Thermomechanical Phenomena in Electronic Systems, IEEE, San Diego, CA, May 30-June 1, pp. 530–538.
[163] Zhang, J., Zhang, R., Schmidt, R., Gilbert, J., Guo, B., 2019, "Impact of Gaseous Contamination and High Humidity on the Reliable Operation of Information Technology Equipment in Data Centers," ASHRAE, Atlanta, GA, Report No. ASHRAE RP-1755.
[164] Singh, P., Klein, L., Agonafer, D., Shah, J. M., and Pujara, K. D., 2015, "Effect of Relative Humidity, Temperature and Gaseous and Particulate Contaminations on Information Technology Equipment Reliability," ASME Paper No. IPACK2015-48176.
[165] Sippola, M. R., 2002, "Particle Deposition in Ventilation Ducts," Lawrence Berkeley National Lab (LBNL), Berkley, CA, Report No. LBNL-52189.